NEUROSCIENCE

Landmark-modulated directional coding in postrhinal cortex

Patrick A. LaChance, Jalina Graham, Benjamin L. Shapiro, Ashlyn J. Morris, Jeffrey S. Taube*

Visual landmarks can anchor an animal's internal sense of orientation to the external world. The rodent postrhinal cortex (POR) may facilitate this processing. Here, we demonstrate that, in contrast to classic head direction (HD) cells, which have a single preferred orientation, POR HD cells develop a second preferred orientation when an established landmark cue is duplicated along another environmental wall. We therefore refer to these cells as landmark-modulated–HD (LM-HD) cells. LM-HD cells discriminate between landmarks in familiar and novel locations, discriminate between visually disparate landmarks, and continue to respond to the previous location of a familiar landmark following its removal. Rats initially exposed to different stable landmark configurations show LM-HD tuning that may reflect the integration of visual landmark information into an allocentric HD signal. These results provide insight into how visual landmarks are integrated into a framework that supports the neural encoding of landmark-based orientation.

INTRODUCTION

Navigation requires a sense of one's orientation in allocentric (world-centered) space (*1*). Head direction (HD) cells in the rodent brain have been suggested to subserve this sense, with each firing preferentially when an animal's head faces a certain allocentric direction (*2*). While the HD signal is vestibular in origin (*3*), its accuracy over time is maintained by referencing external environmental features such as stable visual landmarks (*4*–*6*). This process depends on knowledge of the visual attributes, stability, salience, and spatial distribution of available landmarks, which also provide information about the current spatial context (*7*).

HD-responsive cells have recently been reported in the rat postrhinal cortex (POR) (*8*–*10*), which is the rodent homolog of the human parahippocampal cortex (PHC) (*11*). The PHC is strongly implicated in topographic spatial learning (*12*, *13*) and is activated in response to visual scene (*14*) and landmark (*15*) stimuli. Recording studies in POR have demonstrated responses of single neurons to visual cue changes (*16*) and conjunctions of objects and locations (*17*). POR has reciprocal connections with visual and visuospatial cortical areas (*18*, *19*) as well as the hippocampal formation (*20*, *21*) and preferentially receives subcortical input from the visual thalamus (*22*, *23*) and the HD cell–abundant anterior thalamic nuclei (ATN) (*22*, *24*, *25*). POR is therefore well positioned to integrate information about visual cues with an allocentric HD signal to help anchor an animal's sense of orientation to the outside world (*26*, *27*).

Previous studies of single neurons in the rodent retrosplenial cortex (RSC) (*28*) and medial entorhinal cortex (MEC) (*10*) revealed subsets of HD cells that displayed two preferred firing directions (PFDs; referred to as bidirectional tuning) when two visual cues were present in a two-compartment environment or an open field, respectively. These results were taken to indicate a confluence of visual and HD signals in these brain regions, suggesting an external anchoring of the HD signal by visual properties of the environment. While the PFDs of POR HD cells have been shown to shift along with rotation of a single orienting landmark (*8*), it is not yet known whether the directional responses of POR neurons are directly related to the properties and positions of visual landmarks. POR HD cells may be suited to reference their directional responses to multiple visual landmarks simultaneously, providing a straightforward code for calculating one's orientation relative to visual cues. Such a code could be useful for anchoring the vestibular-dependent HD signal to the outside world before integration with the downstream hippocampal system.

To test this possibility, we recorded from HD-responsive POR cells while rats were exposed to different numbers and positions of prominent visual cues in the environment. Here, we report that, in contrast to classic HD cells in earlier portions of the HD circuit, POR cells that initially respond to a single HD in an environment with one salient landmark cue become bidirectionally tuned when an identical landmark cue is introduced simultaneously elsewhere in the environment, with the second direction depending on the position of the cue. To distinguish these cells from classic HD cells, we refer to them as landmark-modulated–HD (LM-HD) cells. While most LM-HD cells displayed a second peak after introducing the second landmark, other cells, in contrast, displayed a new minimum in their tuning curve, revealing that the firing rates of POR LM-HD cells can be positively or negatively modulated by the presence of prominent visual landmarks. We also found that the firing of POR LM-HD cells is tied specifically to cues that have been previously established as a stable part of the local environment, such that placing an established cue in an unfamiliar location even in the presence of the first cue will elicit firing oriented relative to that location, but a visually distinct cue placed in that location will not. Our results suggest a role for the POR LM-HD signal in processing both HD and visual landmark orientation within the parahippocampal region, as well as information pertaining to the stability of landmark cues within a given environmental context.

RESULTS

The POR LM-HD signal is locked to visual cues

We recorded 87 LM-HD cells in POR (Fig. 1A) from five rats as they foraged for sugar pellets in a square enclosure containing either one or two salient visual cues (identical white cue cards; Fig. 1B). The

Department of Psychological and Brain Sciences, Dartmouth College, Hanover, NH, USA.
*Corresponding author. Email: jeffrey.s.taube@dartmouth.edu

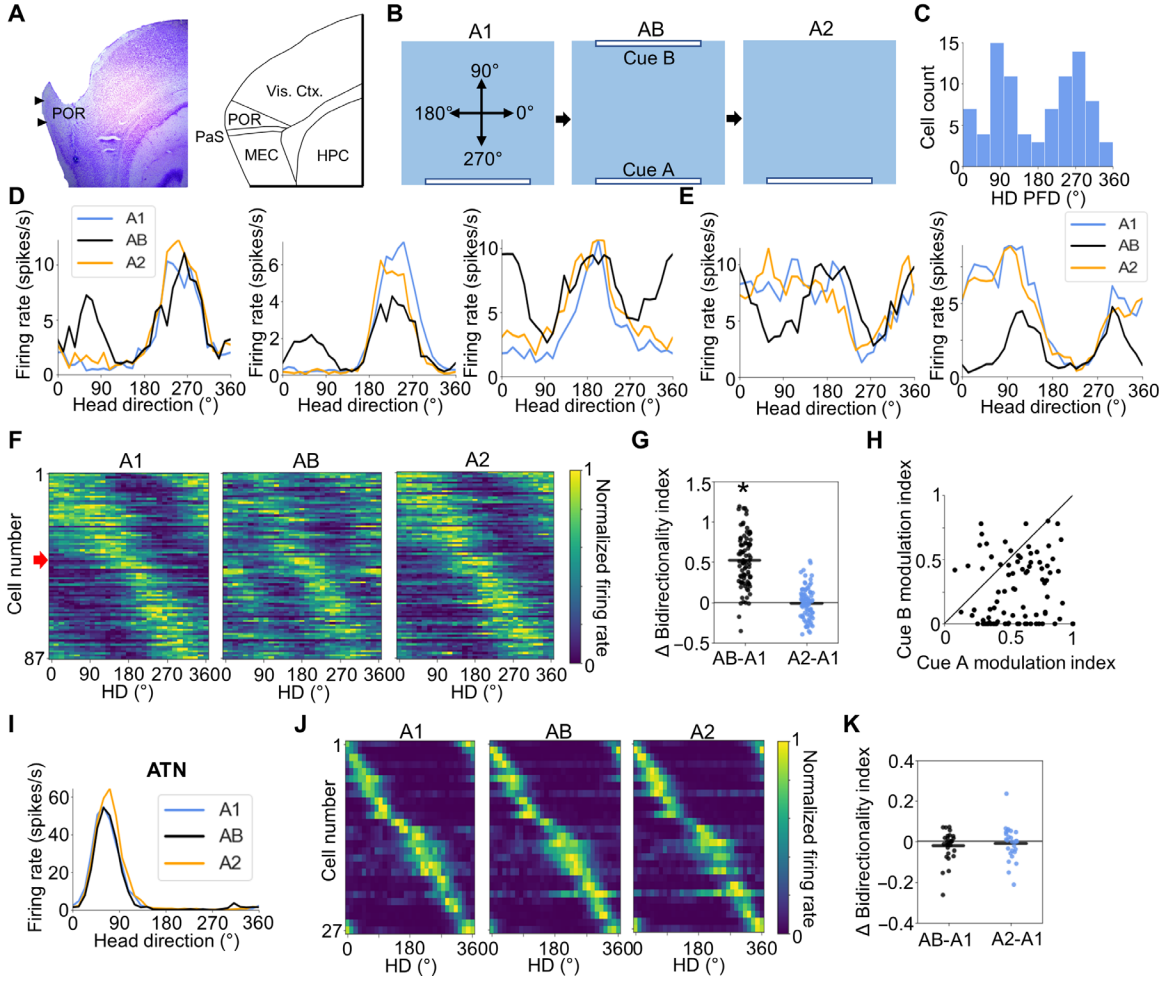

Fig. 1. AB session. (**A**) Left: Nissl-stained sagittal section from one rat showing anatomical borders and cannula track through POR. Right: Atlas diagram showing anatomical borders between brain regions visible in the sagittal section to the left. PaS, parasubiculum; HPC, hippocampus. (**B**) Experimental design for the AB experiment. Top-down view of the recording arena showing the locations of visual cues across A1, AB, and A2 sessions, as well as the reference frame for measuring allocentric HD. (**C**) Histogram of A1 HD PFDs for all 87 POR LM-HD cells recorded in the AB experiment. Note the clustering around 270° (looking toward the cue) and 90° (looking away from the cue). (**D**) Tuning curves for three example POR LM-HD cells recorded across A1, AB, and A2 sessions that showed peak-locked tuning relative to the visual cues. (**E**) Same as (C) but for two LM-HD cells that showed trough-locked tuning. (**F**) Normalized tuning curves for all POR LM-HD cells recorded in the AB experiment. The first 40 cells show trough-locked firing, whereas the remaining 47 are peak-locked; this separation is indicated by a red arrow. (**G**) Comparison of BI between the initial A1 session and both AB and A2 sessions, showing an increase in bidirectionality during the AB session. Asterisk (*) denotes statistical significance. (**H**) Scatter plot depicting the degree of firing rate modulation attributed to cue A or cue B for all POR LM-HD cells recorded during the AB session. Black line shows $x = y$. Note that modulation was generally stronger for cue A than cue B. (**I**) Tuning curves for a representative ATN HD cell recorded across A1, AB, and A2 sessions. (**J**) Same as (F) but for ATN HD cells. (**K**) Same as (G) but for ATN HD cells.

first cue (cue A) was always placed along the south wall (at 270°) and was familiar to the animals by the start of recording because of pretraining sessions. In some recording sessions, in addition to cue A, a second identical cue (cue B) was placed along the north wall (at 90°), which acted as an established cue placed in an unfamiliar location. Distal landmarks were obscured by a circular black curtain surrounding the recording arena from the floor to the ceiling. During an initial recording session with only cue A available (A1 session), the POR LM-HD cells showed unipolar tuning curves with relatively low mean vector lengths (MVLs; mean = 0.301 ± 0.017), wide tuning widths (generally ~180°), and low peak firing rates (mean = 7.212 ± 0.552 spikes/s) compared to neurons typically identified as "classic" HD cells in other brain areas (*2*, *24*, *25*). Consistent with previous studies (*8*, *9*), 65 of the 87 LM-HD cells (75%) were conjunctively tuned to the egocentric bearing of the environment centroid (center-bearing tuning), and 15 of these 87 cells were sensitive to the animal's distance from the centroid (17%; center-distance tuning; fig. S1). Tuning to the centroid may also be considered a proxy for tuning to environmental boundaries (*29*, *30*). Because a given center bearing and a given HD only converge in a restricted portion of the environment, it would be reasonable to expect some of these conjunctive cells to display place fields; however, because of their broad tuning profiles (*8*, *9*) and the relative rarity of distance tuning, allocentric location did not appear to have a dominant influence on the activity of the 87 LM-HD cells given their firing rate heatmaps (fig. S2). Only 25 of these 87 cells (29%) passed a shuffle threshold for significant spatial information content in the A1 session, and only 4 of those 25 spatially modulated cells passed an additional shuffle threshold for border score (see Methods), implying that these cells are overall distinct from place (*31*) or border cells (*32*).

The PFDs of these 87 LM-HD cells showed clustering near 270° (facing toward cue A) and 90° (facing away from cue A; Fig. 1C), unlike the uniform distributions found in traditional HD cell populations (*2*, *24*). We confirmed this by doubling the PFDs to create a unimodal distribution, which would be expected to have a peak at 180° if the original peaks were at 90° and 270°. We found significant clustering near 180° (*V* test: $u = 3.51$, $P = 2.22 \times 10^{-4}$; Rayleigh $r = 0.27$). In a subsequent recording session containing both cues (AB session), the POR LM-HD cells appeared to become bidirectionally tuned, demonstrating two PFDs displaced by 180° (Fig. 1, D to F, and fig. S3, A and B). We used a bidirectionality index (BI; see Methods) to confirm that the sample of POR LM-HD cells became strongly bidirectional during the AB session [BI repeated-measures analysis of variance (ANOVA): $F_{2,172} = 167.21$, $P = 2.57 \times 10^{-30}$; A1 versus AB paired *t* test: $t_{86} = -14.66$, $P = 1.23 \times 10^{-24}$; Fig. 1G]. There was no clear relationship between the LM-HD cells' PFDs and their BI increases in the AB session (fig. S3C). POR LM-HD cells returned to their unidirectional tuning in a subsequent session with only cue A present (A1 versus A2 paired *t* test: $t_{86} = 0.44$, $P > 0.99$; Fig. 1, D to G).

While many LM-HD cells ($n = 47$) maintained a firing rate maximum at their original PFD and added a second maximum 180° opposite during the AB session (that is, the peak of the tuning curve was locked to the presence of a cue: "peak-locked" tuning), other LM-HD cells ($n = 40$) responded differently in the AB session, and it became apparent that these cells were a different type of LM-HD cell. These cells tended to have exceptionally broad tuning curves with a high tonic firing rate that spanned a large portion of the tuning curve (180° to 270°), often without a clear, well-defined peak. The remaining portion of the tuning curve contained a firing rate minimum that could be as sharp as, or sharper than, the maximum. Thus, it was not the high point of the tuning curve but rather the low point that was locked to the cue ("trough-locked" tuning). In the AB session, these cells did not add a second maximum but, instead, a second minimum. This second trough, or reduced firing, occurred 180° opposite the initial trough (Fig. 1E and fig. S3B). We could not distinguish, on the basis of peak firing rates alone in the A1 session, whether cells would show peak- or trough-locked tuning. To determine whether this dissociation (peak versus trough) could be predicted from the cells' A1 session firing properties, we performed a principal components analysis (PCA) on the A1 tuning curves. We found that the first component, which accounted for 44% of the sample variance, separated the cells into two groups (confirmed with *k*-means clustering) according to whether they had a peak (47 of 87 cells) or a trough (40 of 87 cells) near 270°, which was the position of cue A (fig. S4, A and B). We confirmed that these groups showed peak-locked or trough-locked tuning during the AB session, respectively, by comparing their A1 PFDs with their angle-doubled AB PFDs (see Methods). Angle doubling, or multiplying all HDs by 2 before computing tuning curves, has the advantage of turning a bidirectional distribution into a unidirectional one so that regular circular statistics can be applied (*28*, *33*). PFDs for peak-locked cells were aligned between A1 and AB sessions (*V* test for concentration around 0°, $u = 6.64$, $P = 1.55 \times 10^{-11}$; Rayleigh $r = 0.74$), while PFDs for trough-locked cells were displaced in the AB session compared to the A1 session because of insertion of a new firing rate minimum at the cell's previous firing rate maximum (*V* test for concentration around 180°, $u = 2.12$, $P = 0.017$; Rayleigh $r = 0.43$; fig. S4C).

We further modeled the firing of peak-locked and trough-locked cells by fitting both a standard (sharp peak) and inverted (sharp trough) von Mises distribution to the A1 tuning curves and, for each function, compared their R^2 fit values. This analysis produced almost identical clusters to those from the PCA (one cell was switched) and demonstrated that peak-locked cells generally show sharper firing rate maxima than minima (better fits by standard distribution; standard versus inverted R^2 paired *t* test, $t_{46} = 4.25$, $P = 1.06 \times 10^{-4}$), while trough-locked cells showed sharper minima than maxima (better fits by inverted distribution; standard versus inverted R^2 paired *t* test, $t_{39} = -2.62$, $P = 0.012$; fig. S4, D to F). These results suggest that trough-locked cells may actually be inhibited when the animal faces a certain direction, while peak-locked cells are excited (like a typical HD cell) (*2*, *24*, *25*). For this reason, trough-locked LM-HD cells may be considered "anti-HD cells."

To investigate whether cues A and B were encoded similarly during the AB session, we fit a bimodal von Mises mixture to each cell's AB tuning curve and calculated the amount of firing rate modulation that could be attributed to each cue. Cells tended to show a higher modulation index (MI; see Methods) relative to cue A than cue B (paired *t* test, $t_{86} = 8.97$, $P = 5.56 \times 10^{-14}$; Fig. 1H), suggesting that the cue in a more familiar location was more strongly encoded than the less familiar one, possibly related to the perceived stability of that cue placement (*6*, *27*). We additionally investigated whether the more familiar cue location was encoded more consistently over the course of the AB session compared to the less familiar location. We used the correlation of HD tuning curves between the first and second halves of each recording session (split-half correlations) as a measure of tuning stability. While split-half correlations were generally lower in the AB session compared to the A1 and A2 sessions (repeated-measures ANOVA: $F_{2,172} = 10.74$, $P = 4.04 \times 10^{-5}$; A1 versus AB paired *t* test: $t_{86} = 4.49$, $P = 6.50 \times 10^{-5}$; AB versus A2: $t_{86} = -3.36$, $P = 3.52 \times 10^{-3}$; fig. S3D), when we separated the portions of the tuning curves that responded to cue A (within ±90° of the cell's A1 peak or trough) versus cue B (the remaining 180° of the tuning curve), we found no difference in split-half correlations between the two cues (paired *t* test: $t_{86} = 0.18$, $P = 0.86$; fig. S3E). Thus, while tuning stability is somewhat degraded during the AB session, that instability is not uniquely attributable to either cue. We also investigated whether the cells' tuning strengths relative to each cue changed over time by comparing MI values for each cue between the two halves of the AB session. Tuning strength relative to cue A was slightly increased in the second half compared to the first half (paired *t* test: $t_{86} = -2.15$, $P = 0.035$), but tuning strength relative to cue B did not differ across halves ($t_{86} = -0.53$, $P = 0.60$; fig. S3F). Conjunctive center-bearing tuning also did not affect the bidirectional responses of the cells, as LM-HD cells with or without conjunctive center-bearing tuning showed no difference in ΔBI during the AB session (*t* test: $t_{85} = -0.58$, $P = 0.57$; fig. S3G).

Because most of the baseline recording sessions (i.e., A1 sessions) were completed with only cue A present, we might expect that POR LM-HD cells would respond less strongly to cue B after multiple exposures to the AB session because the location of cue A is repeatedly established as more stable. To test for this possibility, we used a linear mixed model to test for changes in BI with repeated exposures to the AB session (fig. S5A). We only used data from animals that had at least two exposures to the AB condition (four animals; PL71, 2 exposures; PL82, 3 exposures; PL86, 5 exposures; and BS6, 10 exposures). The model revealed a significant main effect of exposure ($Z = -4.43$, $P < 0.001$, exposure coefficient = −0.074, 95% confidence interval = [−0.106, −0.041]), such that bidirectional

responses in the AB session decreased with repeated exposures to the AB configuration. This result suggests that POR LM-HD cells may become less sensitive to a stable cue appearing in an unstable location over time. Regardless, even cells recorded after up to 10 exposures to the AB experiment showed higher BIs in the AB session compared to the preceding A1 session, implying that bidirectionality may decrease but does not disappear with experience (fig. S5, A and B). However, it should be noted that electrodes were advanced ventrally between exposures to the AB configuration, and therefore, any effect of exposure could also result from the cells' dorsal-ventral placement in POR.

To determine whether the bidirectional tuning properties were present among classic HD cells in portions of the HD signal circuit closer to where the signal is thought to be generated, we repeated the experiment on 27 HD cells recorded from the ATN (anterodorsal, $n = 2$ rats; anteroventral, $n = 1$ rat). ATN HD cells remained unidirectional across all sessions, including the AB session that contained the two cues (repeated-measures ANOVA: $F_{2,52} = 0.52$, $P = 0.60$; Fig. 1, I to K, and fig. S6A), demonstrating that simultaneous encoding of multiple visual cues is not present early in the HD circuit. The retention of unidirectional tuning in the ATN during the AB session also suggests that the brain maintained an unambiguous sense of allocentric orientation despite the symmetrical landmark configuration and further suggests that this unidirectional representation occurred simultaneously with the bidirectional tuning in POR cells. Consistent with previous findings (*24*, *25*), ATN HD tuning curves tended to have smaller directional firing ranges than those of POR LM-HD cells (mean ATN MVL = 0.71; fig. S6F), and all ATN HD cells showed stronger peaks than troughs in their tuning curves, suggesting that trough-locked tuning is also specific to POR. A sample of HD cells recorded from the MEC and parasubiculum (MEC/PaS; $n = 25$ cells, 4 rats) also remained unidirectional across the A1-AB-A2 sessions ($F_{2,48} = 0.24$, $P = 0.79$; fig. S6, B to D). However, this finding should not be taken to suggest that MEC/PaS HD cells cannot show bidirectional tuning, as some MEC/PaS cells in mice have been reported to become bidirectional in response to certain visual landmark configurations (*10*). In addition, our classification criteria would have likely rejected HD cells that were bidirectionally tuned to begin with. The tuning curves of the 25 MEC/PaS cells showed a range of tuning strengths similar to both the sharply tuned classic ATN HD cells and the broadly tuned POR LM-HD cells (mean MEC/PaS MVL = 0.48; fig. S6F). In sum, the firing and spatial properties of POR LM-HD cells were sufficiently different from classic HD cells in ATN and MEC/PaS that it warrants referring to them using different terminology.

To ensure that there was nothing particular about 180° separation that caused the bidirectional tuning, we recorded 49 POR LM-HD cells from two rats with two white cue cards placed on adjacent walls (cue A at 270° and cue B_{west} at 180°) instead of opposite walls. Session order was A1-AB_{west}-A2 (Fig. 2A). The cells responded to the addition of cue B_{west} by adding a new portion to their tuning curves 90° clockwise from their original peak or trough (Fig. 2, B and C, and fig. S7, A and B). Similar to the initial AB experiment, when we fit a bimodal von Mises distribution to the AB_{west} tuning curve with peaks or troughs separated by 90°, LM-HD cells in the AB_{west} condition were found to be more strongly modulated by cue A than B_{west} (MI paired t test, $t_{48} = 8.10$, $P = 1.60 \times 10^{-10}$; Fig. 2D). Because of the broadness of the LM-HD cell tuning curves in general, the addition of cue B_{west} caused a substantial broadening of the original tuning curves in the clockwise direction (to accommodate the new cue) instead of a discrete secondary peak or trough (Fig. 2, B and C, and fig. S7, A and B). We modeled this broadening by fitting a unimodal von Mises distribution to the tuning curves across the three sessions and comparing the reciprocal of the concentration parameter (1/κ), which is analogous to the variance of a normal distribution (i.e., 1/κ is analogous to σ^2) and increases in

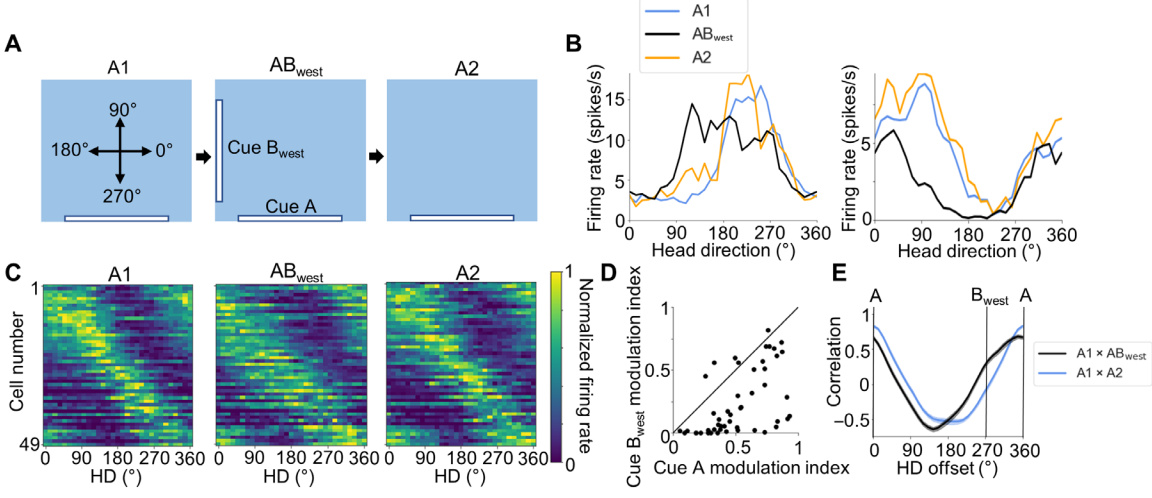

Fig. 2. AB_{west} session. (**A**) Experimental design for the AB_{west} experiment. A top-down view of the recording arena demonstrating the locations of visual cues across A1, AB_{west}, and A2 sessions, as well as the reference frame for measuring allocentric HD. (**B**) Tuning curves for an example peak-locked POR LM-HD cell (left) and a trough-locked POR LM-HD cell (right) recorded across A1-AB_{west}-A2 sessions that showed broadening of their tuning curves in the direction of the new cue location. (**C**) Normalized tuning curves for all POR LM-HD cells recorded across the three sessions of the AB_{west} experiment. (**D**) Scatter plot showing the degree of firing rate modulation that each cell displayed relative to each cue. Note that modulation relative to cue A was generally stronger than to cue B_{west}. Black line shows $x = y$. (**E**) Cross-correlation of tuning curves between A1 and A2 sessions (blue) and between A and B_{west} sessions (black). Note that the A1 × AB_{west} correlations are shifted counterclockwise and show a small bump at 270° corresponding to the location of cue B_{west}. The location of this bump is indicated by the vertical line labeled B_{west}. Error bars show SEMs.

value along with tuning curve width. Tuning curves were significantly wider in the AB_{west} session than the A1 session, as they had increased 1/κ values (repeated-measures ANOVA: $F_{2,96} = 5.60$, $P = 0.005$; A1 versus AB_{west} paired t test: $t_{48} = -2.71$, $P = 0.028$; fig. S7C). The influence of the B_{west} cue can also be observed by cross-correlating the A1 tuning curves with their AB_{west} counterparts; unlike the symmetrical "U" shape obtained by cross-correlating the A1 and A2 tuning curves, the A1-AB_{west} cross-correlation is offset in the counterclockwise direction and shows a small but nondiscrete bump at 270°, which corresponds to the portion of the AB_{west} tuning curve associated with the new cue (Fig. 2E).

POR LM-HD cells encode the previous location of a removed landmark

We next sought to determine whether POR LM-HD representations require direct perception of the visual cue. We recorded 45 POR LM-HD cells from five rats as animals foraged in a square enclosure containing cue A (A1 session) and then in a session without the cue (No cue session; Fig. 3A). Animals were not disoriented between sessions. The cells largely maintained their tuning preferences in the No cue session (V test for PFD shift concentration around 0°, $u = 8.01$, $P = 5.55 \times 10^{-16}$; Rayleigh $r = 0.85$; Fig. 3, B and C, and fig. S8A), suggesting that they retained a memory trace of where cue A was initially located or were at least able to use other cues to maintain their directional preferences, such as remaining sensory elements of the environment, path integration, or attention. As expected, there was no change in bidirectionality across the sessions (BI repeated-measures ANOVA: $F_{2,88} = 2.99$, $P = 0.078$; Fig. 3D). However, the LM-HD cells showed a significant reduction in their tuning strength in the No Cue session (MI repeated-measures ANOVA: $F_{2,88} = 40.31$, $P = 1.36 \times 10^{-11}$; A1 versus No cue paired t test: $t_{44} = 7.07$, $P = 2.75 \times 10^{-8}$; Fig. 3, B, C, and E), indicating that they responded less strongly without direct perception of the cue. Tuning degradation was apparent in both peak-locked and trough-locked LM-HD cells (Fig. 3B and fig. S8B). These responses were not homogeneous, however, as some cells ($n = 29$ with $\Delta MI > -0.2$) largely maintained their tuning properties (Fig. 3F and fig. S8A) while other cells ($n = 16$ with $\Delta MI < -0.2$) showed marked degradation (Fig. 3G and fig. S8B). In addition, the LM-HD cells showed decreased tuning stability across the two halves of the No cue session compared to the A1 and A2 sessions (repeated-measures ANOVA: $F_{2,88} = 40.73$, $P = 1.73 \times 10^{-10}$; A1 versus No cue paired t test: $t_{44} = 7.48$, $P = 6.86 \times 10^{-9}$; No cue versus A2: $t_{44} = -6.33$, $P = 3.30 \times 10^{-7}$; fig. S8C), although their tuning strengths did not differ across halves of the No cue session (MI paired t test: $t_{44} = -0.80$, $P = 0.43$; fig. S8D). Furthermore, whatever loss of tuning strength occurred during the No cue session cannot be attributed to loss of cell recording isolation because POR cells returned to baseline modulation properties in a subsequent A2 session with the cue present (A1 versus A2 MI paired t test, $t_{44} = 0.35$, $P > 0.99$; Fig. 3, B, C, and E). For comparison, ATN HD cells ($n = 28$, three rats) showed no change in firing rate modulation during the No cue session (MI repeated-measures ANOVA, $F_{2,54} = 0.452$, $P = 0.64$; Fig. 3, H and I, and fig. S8, E and F). This latter result is similar to previous findings when recording from HD cells in the postsubiculum (*34*). Collectively, these results again demonstrate the differences between POR LM-HD cells and classic HD cells.

We additionally investigated whether having an AB session immediately preceding the No cue session would cause the POR LM-HD cells to become bidirectional in the No cue session. To test this possibility, we recorded 27 POR LM-HD cells from three rats in the following session order: A1–AB–No cue–A2 (Fig. 3J). We observed the same general pattern as in the AB and No cue experiments (Fig. 3, K to N); LM-HD cells were unidirectionally tuned in the A1 session, became bidirectionally tuned in the AB session (BI repeated-measures ANOVA: $F_{3,78} = 40.68$, $P = 6.27 \times 10^{-16}$; A1 versus AB paired t test: $t_{26} = -8.51$, $P = 3.26 \times 10^{-8}$; Fig. 3N), experienced degraded tuning strength in the No cue session (MI repeated-measures ANOVA: $F_{2,52} = 25.71$, $P = 4.73 \times 10^{-7}$; A1 versus No cue paired t test: $t_{26} = 7.09$, $P = 4.70 \times 10^{-7}$; Fig. 3M), and returned to their baseline unidirectional properties in the A2 session (BI A1 versus A2 paired t test: $t_{26} = 0.27$, $P > 0.99$; MI A1 versus A2 paired t test: $t_{26} = 0.64$, $P > 0.99$; Fig. 3, K to N). The LM-HD cells failed to show a significant increase in bidirectionality in the No cue session compared to the A1 session (BI A1 versus No cue paired t test: $t_{26} = -2.10$, $P = 0.28$) and showed a significant decrease in bidirectionality in the No cue session compared to the AB session (AB versus No cue paired t test: $t_{26} = 7.11$, $P = 8.97 \times 10^{-7}$; Fig. 3N), demonstrating that the bidirectionality present in the immediately preceding AB session was not retained when both cues were removed.

Last, we tested whether the trace responses of POR LM-HD cells to the previous location of a familiar cue could be overshadowed by direct perception of an identical cue in a less familiar location. Of the 87 LM-HD cells recorded in the A1-AB-A2 sessions, we also recorded 39 of them ($n = 5$ rats) as animals foraged in an enclosure containing cue A only (A1 session), followed by a session with cue B only (B session) and then a second session with only cue A (A1-B-A2 session order; Fig. 4A). Note that the B session is similar to a cue rotation session for cue A, although rats were not disoriented in between the sessions as is normally the case for cue rotation experiments. This procedure allowed us to isolate the effects of changes in landmark placement without disrupting other elements of the animals' orientation sense. As we demonstrate below, this aspect has important consequences for how the cells responded in this situation. The population of LM-HD cells overall became bidirectional during the B session (BI repeated-measures ANOVA, $F_{2,76} = 8.82$, $P = 9.87 \times 10^{-4}$; A1 versus B paired t test: $t_{38} = -3.35$, $P = 5.45 \times 10^{-3}$), apparently firing both in response to direct perception of cue B, as well as the previous location of cue A despite its removal (Fig. 4, B to D, and fig. S9A). However, unlike the AB condition where tuning was stronger to cue A, there was no overall difference in firing rate modulation attributable to either of the cues (MI paired t test, $t_{38} = 1.48$, $P = 0.15$; Fig. 4E; also compare Fig. 1D with Fig. 4B), suggesting that firing to the previous location of a familiar cue was overall similar to perception of an identical cue in a less familiar location. Cell responses were not homogeneous, however; while some cells responded similarly to both cues (Fig. 4B and fig. S9A), other cells appeared to "choose" one cue over the other (Fig. 4, G and H, and fig. S9, B to D). Cells could be roughly split according to their firing rate modulation relative to each cue, with 19 of 39 cells preferring cue A ($MI_A - MI_B > 0.2$), 14 of 39 preferring cue B ($MI_B - MI_A > 0.2$), and 6 cells falling somewhere between the two landmarks (Fig. 4E). Cells with different tuning properties could be recorded simultaneously [e.g., cells in Fig. 4 (B and H) were co-recorded; fig. S9D shows six simultaneously recorded LM-HD cells with a variety of responses to the B session]. We separated the tuning curves for cells preferring cue A and those preferring cue B (Fig. 4F) and performed a cross-correlation between the A1 and B tuning curves for each group. The cross-correlation for the cue A group

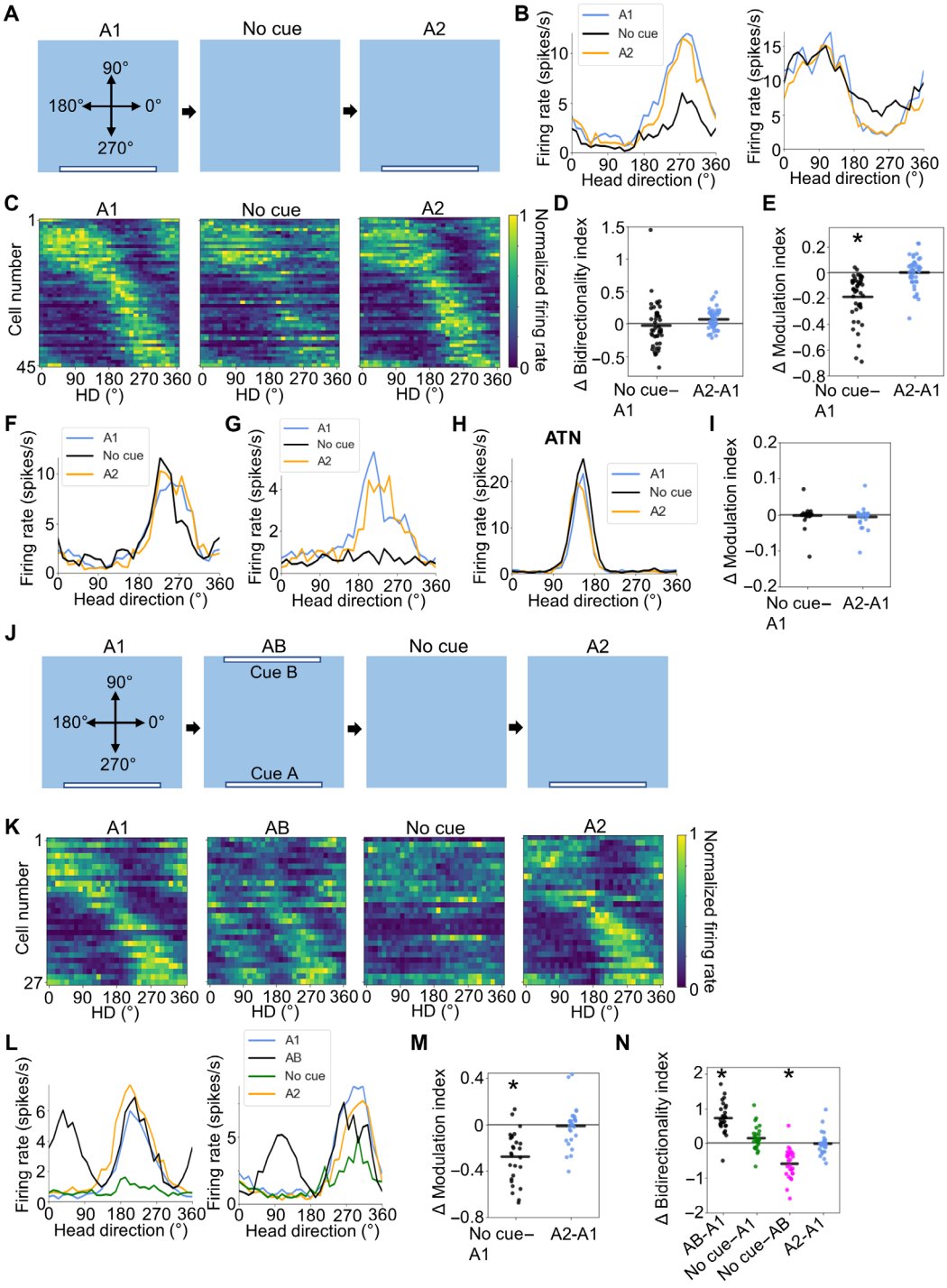

Fig. 3. No cue session. (**A**) Top-down view of the A1–No cue–A2 experiment showing locations of visual cues. (**B**) Tuning curves for an example peak-locked POR LM-HD cell (left) and an example trough-locked cell (right) that reduced their tuning strength when cue A was removed. (**C**) Normalized tuning curves for all POR LM-HD cells recorded in the No cue experiment. (**D**) Comparison of BI between A1 and both No cue and A2 sessions. Note that cells did not become bidirectional during the No cue or A2 sessions. (**E**) Comparison of tuning strength as measured by the MI (see Methods) between the initial A1 session and both No cue and A2 sessions, showing a decrease in modulation during the No cue session. (**F**) Tuning curves for a POR LM-HD cell that stayed strongly tuned across all sessions. (**G**) Tuning curves for an example POR LM-HD cell that showed almost complete tuning degradation during the No cue session. (**H**) Tuning curves for an example ATN HD cell that maintained its firing properties across all sessions. (**I**) Change in MI between the A1 condition and both No cue and A2 conditions for ATN HD cells. (**J**) Experimental design for the A1–AB–No cue–A2 experiment. (**K**) Normalized tuning curves for all POR LM-HD cells recorded in the A1–AB–No cue–A2 experiment. (**L**) Tuning curves for two example peak-locked LM-HD cells. Note that both cells show bidirectionality during the AB session but not during the No cue session where they show unidirectional firing of reduced magnitude. (**M**) Comparison of tuning strength (MI) between the initial A1 session and both No cue and A2 sessions, showing a decrease in tuning strength for the No cue session. (**N**) Comparison of BI between different sessions. Only the AB session displayed increased bidirectionality. Asterisk (*) denotes statistical significance.

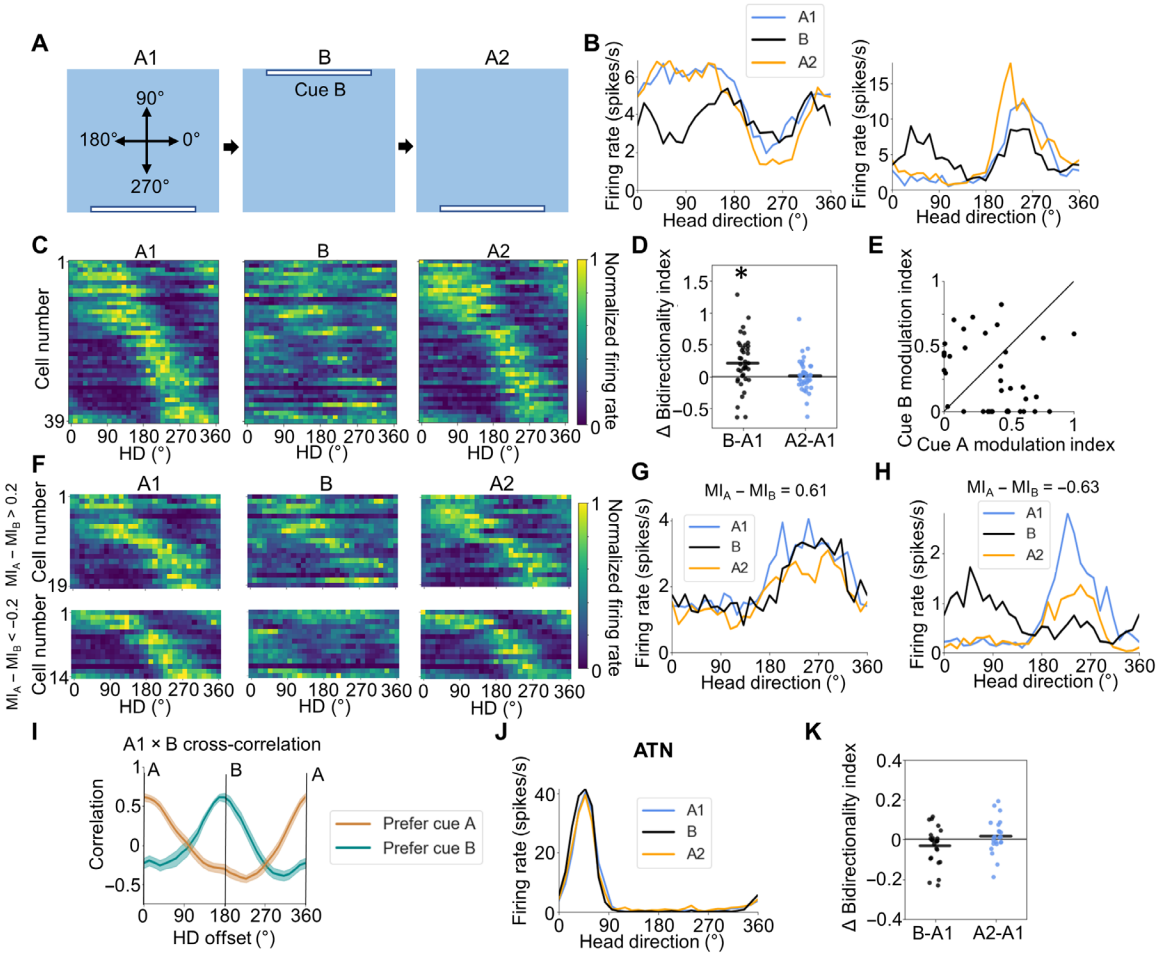

Fig. 4. B session. (**A**) Experimental design for the B experiment. Top-down view of the recording arena showing the locations of visual cues across A1, B, and A2 sessions, as well as the reference frame for measuring allocentric HD. (**B**) Tuning curves for two example POR LM-HD cell that showed trough-locked (left) or peak-locked (right) tuning relative to both cue B and the previous location of cue A. (**C**) Normalized tuning curves for all POR LM-HD cells recorded in the B experiment. (**D**) Comparison of BI between the initial A1 session and both B and A2 sessions, showing an increase in bidirectionality during the B session. Asterisk (*) denotes statistical significance. (**E**) Scatter plot comparing the degree of firing rate modulation attributed to cues A and B during the B session for all recorded POR HD cells. Black line shows $x = y$. (**F**) Normalized tuning curves for LM-HD cells recorded during the B experiment that have been split according to whether their firing during the B session mostly favors cue A ($MI_A - MI_B > 0.2$), upper row or cue B ($MI_A - MI_B < -0.2$), lower row. (**G**) Tuning curves for an example POR LM-HD cell that remained tuned to cue A across all sessions. (**H**) Tuning curves for an example POR LM-HD cell that switched to mainly encoding cue B during the B session. (**I**) Cross-correlation between A1 and B session tuning curves, split according to the groupings in (F). Note that cells preferring cue A show a peak near 0°, while cells preferring cue B show a peak near 180° (**J**) Tuning curves for an example ATN HD cell that maintained its firing properties across all sessions. (**K**) Change in bidirectionality from session A1 to sessions B and A2 for ATN HD cells.

showed a maximum correlation at 0° offset and a minimum near 180°, suggesting consistent tuning preferences between the A1 and B sessions, while the cue B group showed a peak near 180° and a minimum near 0° (Fig. 4I), demonstrating that those cells became tuned to the opposite direction in the B session.

Tuning curve correlations were lower between both halves of the B session compared to the A1 and A2 sessions (repeated-measures ANOVA: $F_{2,76} = 32.41$, $P = 1.23 \times 10^{-7}$; A1 versus B paired t test: $t_{38} = 6.52$, $P = 3.29 \times 10^{-7}$; B versus A2: $t_{38} = -4.99$, $P = 4.10 \times 10^{-5}$; fig. S9E), although the portion of the tuning curves related to cue B was no less stable than the portion related to cue A (paired t test, $t_{38} = -1.21$, $P = 0.23$; fig. S9F). There was also no significant change in tuning strength relative to cue A in the first half versus the second half of the session (MI paired t test: $t_{38} = -0.84$, $P = 0.41$; fig. S9G), although there was a small overall decrease in tuning strength relative to cue B in the second half (MI paired t test: $t_{38} = 2.32$, $P = 0.026$). However, this response was only found to be the case for cells that did not prefer cue B overall (i.e., full session $MI_B - MI_A < 0.2$; B-preferring cells, $t_{13} = 1.07$, $P = 0.30$; non–B-preferring cells, $t_{24} = 2.07$, $P = 0.050$; fig. S9G), which may have encoded cue B more strongly in the first half of the session. POR LM-HD cells returned to displaying their unidirectional tuning properties in a subsequent A2 session (A2 versus A1 BI paired t test, $t_{38} = -0.35$, $P > 0.99$; Fig. 4, B to D). In contrast to POR LM-HD cells, ATN HD cells ($n = 24$ cells, 3 rats) remained unidirectional (BI repeated-measures ANOVA, $F_{2,46} = 1.95$, $P = 0.15$) and maintained their PFDs between A1 and B sessions (V test for concentration around 0°, $u = 23.87$, $P = 2.78 \times 10^{-12}$; Rayleigh $r = 1.0$; Fig. 4, J and K, and fig. S9, H and I), reinforcing the view that these bidirectional properties are not present among classic HD cells early in the HD signal generation circuit. In

addition, the consistent tuning of ATN HD cells suggests that the B-only session was not treated by the brain as a simple cue rotation experiment [see (*5*, *24*)], and unambiguous directional information (via sensory or vestibular cues) was available to the animal during this session.

POR LM-HD cells discriminate between visually disparate cues

Having demonstrated that POR LM-HD cells respond bidirectionally to a pair of identical visual cues, we sought to determine whether they respond similarly when the cues have distinct visual properties. We recorded 36 POR LM-HD cells as rats ($n = 4$) foraged in a square enclosure containing either cue A (A1 session) or both cue A and a black cue card (cue C) placed along the north wall (AC session; Fig. 5A). Overall, POR cells maintained their unidirectional tuning properties between the two conditions (BI repeated-measures ANOVA, $F_{2,70} = 1.00$, $P = 0.37$; Fig. 5, B to E, and fig. S10A), suggesting that they strongly discriminated between the visually disparate cues. However, 2 of the 36 cells (6%) did show clear bidirectional tuning in the AC condition (Fig. 5F, right; fig. S10B), indicating that POR cells may have the capacity to generalize across visually distinct cues. Cells with these two types of responses could be co-recorded within the same session (Fig. 5F), which suggests that different POR LM-HD cells may be performing different functions. In addition, two LM-HD cells (from different animals but co-recorded with stable unimodal LM-HD cells) showed a large increase in firing rate near 90° during the AC session, regardless of their A1 or A2 PFDs (fig. S10C), which may further indicate encoding of cue C by POR cells. These heterogeneous responses further indicate that a single attractor network is unlikely to account for the firing properties of all POR LM-HD cells. However, a small number of example cells alone cannot definitively prove that a substantial portion of POR LM-HD cells responds to visually unfamiliar cues, and further studies will be necessary to determine whether such a subpopulation exists. Split-half correlations were no lower in the AC session than in the A1 session (repeated-measures ANOVA: $F_{2,70} = 5.41$, $P = 0.012$; A1 versus AC paired t test: $t_{35} = 1.46$, $P = 0.46$; fig. S10D), suggesting that the addition of cue C (an unfamiliar cue in an unfamiliar location) did not disrupt the cells as much as cue B (a familiar cue in an unfamiliar location) in the previous experiments.

Effects of experience with different initial cue configurations

All the experiments outlined thus far have recorded POR LM-HD cells from rats that were initially habituated to an environment with a single white landmark cue (cue A). It is possible, however, that HD-responsive cells in POR would show different responses in animals that were initially familiarized to environments with different numbers or types of cues. To investigate this issue, we recorded POR LM-HD cells from three groups of rats ($n = 3$ rats each) that were initially habituated to either (i) a black cue card along the south wall (black-cue condition), (ii) two white cue cards along the north and

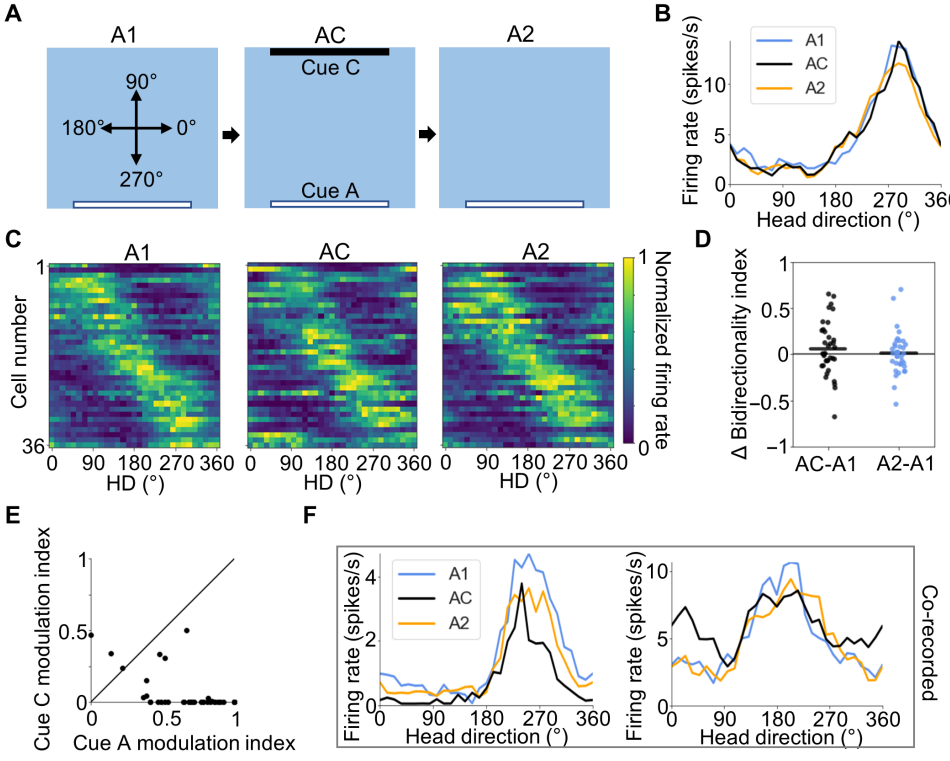

Fig. 5. AC session. (**A**) Experimental design for the AC experiment. Top-down view of the recording arena showing the locations of visual cues across A1, AC, and A2 sessions, as well as the reference frame for measuring allocentric HD. (**B**) Tuning curves for an example POR LM-HD cell recorded across A1, AC, and A2 sessions that did not respond to the addition of cue C. (**C**) Normalized tuning curves for all POR LM-HD cells recorded in the AC experiment. (**D**) Comparison of BI between the initial A1 session and both AC and A2 sessions, showing no change in bidirectionality in either session. (**E**) Scatter plot comparing the degree of firing rate modulation attributed to cues A and C during the AC session for all recorded POR LM-HD cells. Black line shows $x = y$. Note that cells largely showed stronger tuning to cue A than cue C. (**F**) Tuning curves for two co-recorded POR LM-HD cells, one of which did not respond to the addition of cue C (left) while the other became bidirectional (right); note the increase in firing rate around 30°.

south wall (two-cue condition), or (iii) no cue cards at all (No cue condition). Of 70 total POR cells recorded in the black-cue condition (group 1), 30 were classified as LM-HD cells (43%), a similar proportion to those found in animals trained with a white cue [50%; see Methods; $\chi^2(1) = 1.24$, $P = 0.27$]. These cells showed a similar PFD distribution to those recorded in the initial AB experiment, with apparent peaks near 270° and 90°, although a *V* test on doubled PFDs did not reveal significant clustering ($u = 1.21$, $P = 0.11$; Fig. 6E). We recorded 24 of these cells in a series of three recording sessions that mirrored the initial AB experiment (A1 black–AB black–A2 black; Fig. 6A). Much like the initial AB experiment, the LM-HD cells recorded in the black cue condition became significantly bidirectional in the AB black session compared to the A1 black session (BI repeated-measures ANOVA: $F_{2,46} = 19.79$, $P = 6.89 \times 10^{-6}$; paired *t* test: $t_{23} = -5.61$, $P = 3.12 \times 10^{-5}$; Fig. 6, B to D), suggesting that familiarity with the landmark cue drives bidirectionality among the LM-HD cells, not the color of the cue. There was also a small increase in bidirectionality in the A2 session compared to the A1 session (A1 versus A2 paired *t* test: $t_{23} = -3.21$, $P = 0.012$), although cells were less bidirectional than in the AB session (AB versus A2: $t_{23} = 3.50$, $P = 5.77 \times 10^{-3}$; Fig. 6D); thus, this increase is likely a result of natural variability and not a tuning feature of the cells per se.

When the rats were initially trained in the two-cue (AB) condition (group 2), we initially suspected that a large proportion of POR LM-HD cells would be bidirectionally tuned to begin with, as the animals had been exposed only to an environment with two identical oppositely placed cues. Instead, the directionally tuned cells that we observed were largely unidirectional; of 108 POR cells recorded in the two-cue condition, 71 were classified as HD-responsive cells (66%) on the basis of assumptions of a unidirectional tuning curve (see Methods). This proportion is higher than the 50% observed among POR cells of animals trained with a single white cue card [$\chi^2(1) = 8.10$, $P = 0.0044$]. The prevalence of unidirectional tuning suggests that the largely bidirectional firing displayed by LM-HD cells in the original AB experiment was mainly the result of seeing a familiar cue in an unfamiliar location because having two familiar cues in familiar locations did not elicit strong bidirectionality. Somewhat unexpectedly, the PFDs of these unidirectionally tuned cells were not oriented toward the cues (*V* test on doubled PFDs for clustering near 180°: $u = -0.54$, $P = 0.71$; Fig. 6J). This result supports the hypothesis that POR LM-HD cells are not simply reacting to the visual presence or absence of a landmark cue but rather using the available stable cues to calculate a reasonable orientation signal. Of the 71 LM-HD cells recorded in the two-cue condition, we recorded 66 of them in a series of recording sessions that started with an AB session, after which we removed cue B, and lastly ended with another AB session (AB1-A-AB2). We observed no change in the bidirectionality of the cells when cue B was removed (BI repeated-measures ANOVA: $F_{2,130} = 0.76$, $P = 0.47$; Fig. 6I) and no change in tuning strength (MI repeated-measures ANOVA: $F_{2,130} = 1.54$, $P = 0.22$), suggesting that the cells were able to use cue A and other remaining orienting information to preserve their directional preferences and tuning strengths.

Despite the fact that LM-HD cells in the two-cue condition were largely unidirectional, visual inspection of the tuning curves suggested that many of the cells actually had a small bidirectional component (i.e., a small peak or trough 180° opposite the main one). Because the second peak or trough was generally much smaller than the primary peak or trough, this effect is not apparent in Fig. 6H. We compared the distribution of BI values for the 66 cells recorded in the baseline session (AB1) of the two-cue condition to those of the 87 cells recorded in the baseline session (A1) of the original AB experiment. While the cells trained with one cue showed an A1 BI concentration near a value of −0.4 (representing much stronger unimodal than bimodal tuning), cells trained with two cues showed a peak near −0.4, as well as a second peak closer to 0 (fig. S11A). This second peak may represent cells with a small bidirectional component. We compared the one-cue and two-cue distributions using a Mann-Whitney *U* test ($U = 2177$, $P = 0.0053$), which showed that they differed. We then looked specifically at two-cue cells that had BI > −0.2 in the AB1 session, which accounted for 25 of the 66 cells (38%). Tuning curves for those cells tended to have a small secondary peak or trough that persisted across the AB1-A-AB2 series (fig. S11C). In agreement with this observation, there was no overall difference in bidirectionality across the sessions (BI repeated-measures ANOVA, $F_{2,48} = 0.066$, $P = 0.94$; fig. S11B), suggesting that the tuning preferences of these cells were retained despite removal of one cue. Thus, while HD-responsive cells in the POR of animals trained with two identical cues are largely unidirectional, some still retain a small bidirectional component.

In addition, we wanted to determine whether HD-like responses are observable in the POR of animals that have only been exposed to an enclosure with no cue cards at all. Thus, following training in an enclosure without any cues (at least seven exposures before recording), we found that of 145 cells, 35 (24%) were classified as having a significant unidirectional response to the animal's HD, demonstrating that HD-like signals exist in POR without the presence of salient visual cues, although at a lower proportion of cells than those of animals trained with one white cue card [$\chi^2(1) = 28.43$, $P = 9.73 \times 10^{-8}$]. These cells did not show a clearly biased PFD distribution (Fig. 6O) and were not oriented toward the typical location of cue A or cue B as in previous experiments (*V* test on doubled PFDs for clustering near 180°: $u = 0.072$, $P = 0.47$). For 29 of these cells, we ran a subsequent recording session in which we introduced a pair of visually identical cue cards along the north and south walls (AB session). The pairs of cue cards used on each subsequent recording day were visually distinct to avoid them being learned as "stable cues" (i.e., two white cue cards on day 1, two black cue cards on day 2, two vertically striped cue cards on day 3, etc.; see Methods). If directionally responsive neurons in POR cared about the presence of visual landmarks without regard for their stability or familiarity, then we would expect to see a bidirectional response in the AB session. Instead, the cells remained unidirectional when both cues of any appearance were present (BI repeated-measures ANOVA: $F_{2,56} = 5.10$, $P = 0.009$; no pairwise differences between AB and No cue sessions; Fig. 6, L to N), reinforcing the view that directional responses in POR are only tied to landmark cues if they have already been established as a stable element of the local environment.

Last, we wanted to determine whether the POR cells trained in the No cue condition could still use the two unfamiliar cues to reset their orientation preferences. For 17 of the cells recorded in the No cue 1–AB–No cue 2 experiment, we followed the second No cue session by disorienting the animal and then placing it into the enclosure with the two cue cards placed on the east and west walls of the enclosure rather than the previous north and south wall locations (AB 90° rotated session). This session was followed by a final AB session with the cues back on the north and south walls (fig. S12A). POR HD-responsive cells tended to rotate their PFDs in the

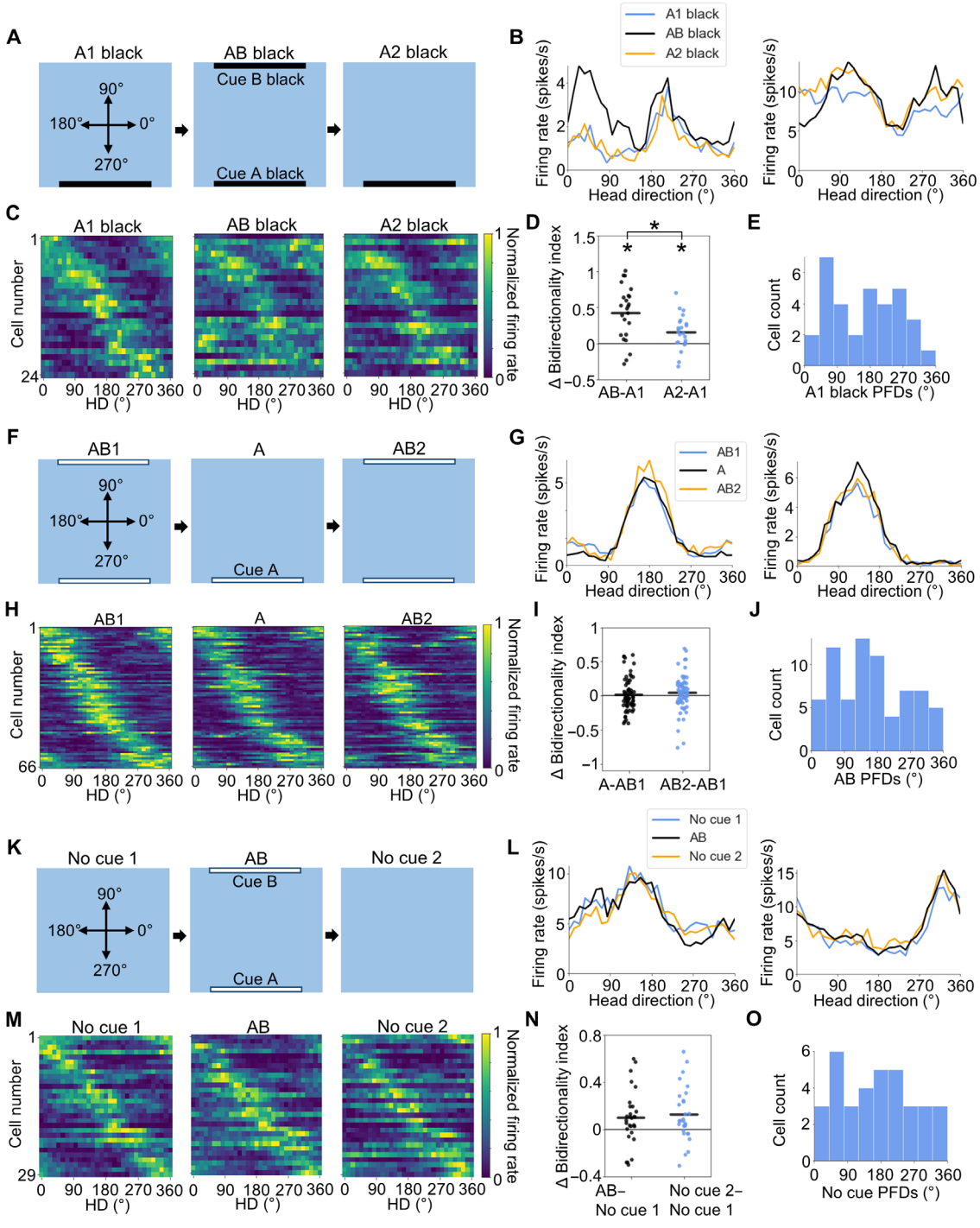

Fig. 6. Effects of habituation to different cue configurations. (**A**) Experimental design for the AB black experiment. Top-down view showing the locations of visual cues across A1 black, AB black, and A2 black sessions. (**B**) Tuning curves for two example POR LM-HD cells from the AB black experiment that showed bidirectional tuning in the AB black session. (**C**) Normalized tuning curves for all POR LM-HD cells recorded in the AB black experiment. (**D**) Comparison of BI between A1 black and both AB black and A2 black sessions. Asterisk (*) denotes statistical significance. Note that bidirectionality was increased in the AB black session relative to both A1 black and A2 black sessions, although it was slightly elevated in the A2 black session. (**E**) Distribution of HD PFDs for all LM-HD cells recorded in the A1 black session. (**F**) Experimental design for the AB1-A-AB2 experiment. (**G**) Tuning curves for two example POR LM-HD cells recorded across the sessions of the AB1-A-AB2 experiment that showed largely unidirectional tuning in all sessions. (**H**) Normalized tuning curves for all POR LM-HD cells recorded in the AB1-A-AB2 experiment. (**I**) Comparison of BI between AB1 and both A and AB2 sessions. (**J**) Distribution of HD PFDs for all LM-HD cells recorded in the AB1 session. (**K**) Experimental design for the No cue 1–AB–No cue 2 experiment. (**L**) Tuning curves for two example POR LM-HD cells recorded across the sessions of the No cue 1–AB–No cue 2 experiment that showed unidirectional tuning in all sessions. (**M**) Normalized tuning curves for all POR LM-HD cells recorded in the No cue 1–AB–No cue 2 experiment. (**N**) Comparison of BI between No cue 1 and both AB and No cue 2 sessions. (**O**) Distribution of HD PFDs for all LM-HD cells recorded in the No cue 1 session.

AB rotated condition following disorientation (mean absolute rotation = 67.71°; *V* test for concentration near 90°: $u = 4.35$, $P = 6.66 \times 10^{-6}$; Rayleigh $r = 0.80$; fig. S12, B and C), although some cells did not shift their PFDs (6 of 17 cells with PFD shifts <45°; fig. S12D). Thus, while the cells can use the relatively unfamiliar cues to orient themselves when few other orienting cues are available, in some cases, the cells may rely on other uncontrolled cues that are deemed more stable. Cells co-recorded in a single session either rotated or did not rotate coherently (five sessions with rotation and three sessions without); thus, it is possible that the disorientation process was insufficient in some cases to fully disorient the animal. PFDs were consistent between the first and final sessions (mean shift = 0.77°; *V* test for shift concentration near 0°: $u = 5.34$, $P = 4.65 \times 10^{-8}$; Rayleigh $r = 0.92$).

DISCUSSION

POR LM-HD cells appear to lock their directional preferences to stable visual landmarks such that they display bidirectional firing when a stable landmark cue is duplicated on a wall 180° opposite in a single environment. Unlike HD cells found in other brain areas (*2*, *24*, *25*), POR LM-HD cells either lock their maximum firing rate (peak-locked) or minimum firing rate (trough-locked) to the cue, which is indicated by whether the cell has a peak or trough in its tuning curve near where the animal's HD aligns with the normal vector from the cue. Firing to each cue depends on the animal's familiarity with the cue and its current location relative to its usual location such that greater firing rate modulation is observed relative to a cue in a stable location. These cells maintain their PFDs but show a decrease in their tuning strength when the familiar cue is removed from the environment, suggesting that their firing is modulated by, but not fully dependent on, direct perception of the cue. POR LM-HD cells also discriminate between visually distinct cues. However, when two identical visual cues are present from the start of habituation to the environment, HD-responsive POR cells show largely unipolar tuning curves, suggesting that POR can use multiple stable landmarks simultaneously to develop an accurate sense of orientation.

Cells with bidirectional tuning properties have also been reported in RSC (*28*), with which POR shares reciprocal connections (*18*, *19*). However, RSC bidirectional cells only showed this tuning in a specific multicompartment environment, and the subset of cells showing bidirectional tuning within a single compartment did not show directional tuning in an open field (*28*). In contrast, POR cells can show both unidirectional and bidirectional tuning in a simple open-field environment, depending on the cues that are present. Furthermore, in another experiment with RSC and postsubiculum HD cells, no evidence was found for bidirectional tuning in an open-field environment with two oppositely placed identical cues (*33*). A subset of HD cells in the mouse MEC (which is directly downstream from POR) and PaS have been reported to show bidirectional tuning in an environment with multiple visual landmark cues (*10*). However, unlike HD cells in the current study, the number and orientations of the PFDs displayed by the MEC cells were not directly bound to the number and positions of landmarks, respectively (*10*). Nonetheless, given the close anatomical connectivity between the two areas, it is possible that some portion of the landmark-modulated firing observed among MEC HD cells is inherited from the POR (*21*). In addition, bidirectional cells found in the RSC (*28*) and MEC/PaS (*10*) could be co-recorded with classic HD cells that did not show the reported bidirectional properties. This situation does not seem to be the case with our POR LM-HD cells, and we do not see strong evidence for a separate population of classic HD cells in POR. Even cells with more classic tuning curves (e.g., the leftmost two example cells in Fig. 1D) became bidirectionally tuned in the AB session.

One unexpected finding was that, unlike traditional HD cells, which increase their firing rates when the rat's head points in a particular direction (*2*), POR LM-HD cells can either increase their firing rates (peak-locked cells) or decrease their firing rates (trough-locked or anti-HD cells). POR LM-HD and anti-HD cells may represent a conjunction between visual inputs (*19*, *22*, *23*) representing visual properties of the cue and vestibular-based HD inputs from the ATN (*3*, *22*, *24*, *25*). It is possible that the peak-locked cells receive convergent excitatory input from visually tuned cells and HD cells, while trough-locked cells receive inhibitory input, although further research will need to address how visual and HD inputs converge upon POR cells. POR cells in head-fixed mice have been shown to respond to visual cues (*23*), and visual response properties have been suggested to contribute to the encoding of stimulus identity in the mouse POR (*35*). Cells conjunctively encoding allocentric HD with the egocentric bearing of a visual cue have also been reported in the posterior parietal cortex (*36*), with which POR is connected (*18*, *19*). These types of cells may play a role in anchoring the brain's HD representation to visual cues (*26*, *27*).

Our finding that POR LM-HD cells maintained their PFDs when cue A was removed (No cue session) suggests that their firing was not entirely dependent on direct perception of the landmark. One possible explanation is that they were able to use remaining visual properties of the enclosure (e.g., corners and specific folds in the surrounding curtain) to maintain their tuning. However, we have previously shown that POR HD cells maintain their PFDs in complete darkness (*8*), so remaining visual cues in the environment do not appear to be absolutely necessary for maintained directional tuning. Alternatively, the cells could have relied on path integration, maintaining their sense of orientation between the A1 and No cue sessions by keeping track of head turns, possibly via projections from brain areas that contain more classic, vestibular-driven HD cells (e.g., the ATN) (*22*, *24*, *25*). In addition, attentional, representational, or mnemonic processes likely contribute to the maintained firing, with the true resolution to this issue likely being a mixture of these processes depending on the available cues. Further work will be necessary to determine exactly how visual and vestibular-based signals are integrated in POR.

An argument could also be made that POR LM-HD cells cannot support unambiguous directional processing if they respond similarly to symmetrically placed visual landmarks; that is, when two identical landmarks are placed along the north (90°) and south (270°) walls of the enclosure, the POR HD cells apparently cannot differentiate between north and south, firing in both directions. However, POR LM-HD cells did differentiate between the two directions by modulating their firing rates more strongly relative to one cue location than the other cue location (Fig. 1H), with firing to the second cue becoming less strong with repeated exposures to the AB condition (fig. S5). Bidirectional firing in this manner has been suggested to communicate information about the relative stability of each cue and its location (*27*), providing the HD system with a sense of how reliable the location of each available landmark is. It is clear that unambiguous directional information was available to the brain during the AB experiment, as ATN HD cells maintained their unidirectional firing

properties with both cues present. In addition, when two identical cues were available to the animals from the beginning of the experiment (two-cue condition), POR cells generally showed unidirectional tuning curves (although often with a small bidirectional component), suggesting that POR has access to unambiguous directional information despite environmental symmetry. The unidirectional firing properties of LM-HD cells in the two-cue condition are similar to the properties of "abstract landmark bearing" cells predicted to lie upstream of RSC, which may encode a unidirectional HD signal based on the conjunctive egocentric bearings of all visual landmark cues, although our POR cells are more broadly tuned than these cells were predicted to be (*37*). This unidirectional firing also suggests that the bidirectional responses observed in the original AB session were the result of observing a single stable landmark cue in a second location rather than a separate orientation signal defined relative to each cue individually. It is possible that, for animals trained with two identical cues from the beginning, directional POR cells were initially bidirectional but became unidirectional with repeated habituating exposures to the environment before neural recordings. Further studies investigating the development of the signal in different environments will be necessary to determine whether this possibility is true.

The POR has previously been implicated in the processing of contextual information. Recording experiments have indicated that POR neurons change their spatial representations following visual cue changes (*16*) and are responsive to conjunctions of objects and locations (*17*), both of which may be related to the differential responses of POR LM-HD cells to visual cue configurations in the current study. The POR has also been implicated in processing item-place representations related to macroscale (e.g., large landmark cues) but not microscale (e.g., small objects) items (*38*), which is consistent with our results demonstrating landmark-place responses among POR LM-HD cells related to large visual landmark cues. In addition, lesion studies have directly implicated POR in contextual processing, with POR lesions impairing contextual learning (*39*) and context discrimination (*40*). POR LM-HD cells may contribute to contextual encoding in the downstream entorhinal cortex and hippocampus (*41*). Given POR's early position in the medial temporal lobe processing stream, one could speculate that POR responses play a role in the neural manifestation of spatial context as information is funneled toward the hippocampus. Although some of our results could be interpreted to show that the POR supports spatial context discrimination by indicating the types and locations of available cues, this view is difficult to reconcile with our findings that (i) bidirectionality decreased over repeated exposures to the AB cue configuration and (ii) cells of animals trained with two identical cues from the beginning were largely unidirectional, making this property less conducive for establishing the current spatial context. Instead, POR LM-HD cells may implicitly represent spatial context by calculating an HD estimate based on visual landmark cues that have been established as stable elements of a given environment. Our results also agree with lesion studies implicating the POR in orienting (*42*) and visual discrimination (*43*, *44*) behavior and may relate to cue-related firing found throughout the hippocampal formation (*10*, *45*–*48*). However, the POR is unlikely to be a major source of visual landmark information for earlier stages of the HD circuit (e.g., in the ATN) (*49*), which could be conveyed by the postsubiculum (*50*, *51*).

Further studies will be necessary to determine how POR LM-HD cells are affected by different types and combinations of visual cues. For example, it would be interesting to repeat these experiments using distal cues to determine whether the LM-HD cells treat them similarly to local cues or under circumstances where both distal and local cues are available to the animal. Similarly, it would be interesting to determine how these cells respond in a more complex local environment, such as one that contains two or more visually disparate cues from the beginning (i.e., both a black and white cue card) or one that contains both small-object and large-landmark cues.

In addition to the cue-responsive directional signals reported here, cells in POR have been reported to encode the egocentric bearing and/or distance of the environment center or boundaries (fig. S1) (*8*, *9*). A landmark-based HD signal in POR may provide a means to anchor this egocentric representation to an allocentric reference frame for mapping space and directing vector-based navigation (*52*, *53*), as well as differentiating between different maps according to the positions of stable landmarks that have been previously associated with each environment (*53*).

Our results align with a recent recording study in the human PHC, which found that neurons representing allocentric HD showed a bias toward a prominent peripheral landmark (*54*). The allocentric tuning of these PHC "direction" cells was distinct from egocentric tuning to locations within the arena (*54*). Similarly, while we found that many POR LM-HD cells were conjunctively tuned to egocentric center bearing, center-bearing tuning appears to be independent from the cells' landmark-related firing properties (fig. S3G). Parallels between these studies represent steps toward understanding the role of the PHC/POR in guiding topographic learning and navigation (*12*), as well as deficits associated with PHC damage such as topographical disorientation (*13*). Overall, our study provides insights into how sensory properties of visual cues are integrated into an allocentric spatial framework to support a sense of orientation within the mammalian brain.

METHODS

Subjects

Subjects were 25 female Long-Evans rats aged 5 to 7 months at the start of testing. Rats were individually housed in Plexiglas cages and maintained on a 12-hour light/12-hour dark cycle. Before surgery, food and water were provided ad libitum. All experimental procedures involving the rats were performed in compliance with institutional standards as set forth by the National Institutes of Health *Guide for the Care and Use of Laboratory Animals* and approved by the Dartmouth Institutional Animal Care and Use Committee (*8*).

Electrode construction

Animals were implanted with a movable microdrive consisting of a bundle of four tetrodes targeting the POR (22 rats) or a bundle of eight stereotrodes targeting the anterior thalamus (ATN; 3 rats). The stereotrodes or tetrodes were constructed by twisting together two or four strands of 17-μm nichrome wire, respectively. These twisted strands were subsequently threaded through a single 26-gauge stainless steel cannula, and the end of each wire was connected to a single pin of a Mill-Max connector. The two center pins of the connector were attached to the cannula, which acted as an animal ground. Three drive screws were secured around the connector using dental acrylic, making the electrode drivable in the dorsal-ventral plane (*8*).

Electrode implantation

Animals were anesthetized with isoflurane. They were subsequently placed in a stereotaxic frame, and an incision was made in the scalp to expose the skull. A single craniotomy was drilled above the target structure. Implant coordinates were as follows: POR, 0.45 mm anterior to the transverse sinus, 4.6 mm lateral to lambda, and 1 mm ventral to the cortical surface and ATN, 1.3 mm lateral to bregma, 1.5 mm posterior to bregma, and 3.7 mm ventral to the cortical surface. For POR implants, the tetrode tips were also angled 10° forward in the sagittal plane such that the tetrode tips were pointing anteriorly. All electrodes were secured to the skull using dental acrylic (*8*). Two of the POR-implanted animals additionally had infusion cannulae implanted above the anterior thalamus as part of a separate experiment.

Recovery and behavioral training

Rats were allowed 7 days to recover from surgery, after which they were placed on food restriction such that their body weight reached 85 to 90% of its presurgical level. During this time, the rats were also trained to forage for randomly scattered sucrose pellets within a gray square box (either 100 cm by 100 cm or 120 cm by 120 cm; 50 cm in height) surrounded by a uniform black curtain that formed a circle around the square box. While the box itself was featureless, we trained four groups of rats, with each group habituated to different numbers and types of visual cues placed along the inside walls of the box. The different groups were as follows: (i) a single white cardboard sheet placed along the south wall (cue A; n = 13 POR rats, n = 3 ATN rats), (ii) a single black cardboard sheet placed along the south wall (cue A black; n = 3 POR rats), (iii) two white cardboard sheets placed along the south (cue A) and north (cue B) walls (n = 3 POR rats), and (iv) no landmark cues (n = 3 POR rats). Cue cards were 50 cm in height (such that they covered the full vertical extent of the wall) and had a width of 60 cm for the 100-cm box and 72 cm for the 120-cm box, such that they covered 60% of the horizontal extent of the wall. In all cases, the floor was composed of gray photographic backdrop paper. Recording began when the animals' walking paths showed uniform coverage (>80%) of the entire arena during 20- or 10-min sessions in the 120- or 100-cm enclosures, respectively (*8*).

Recording of neural data

Over the course of weeks to months, tetrodes or stereotrodes were "screened" for cells as the animals foraged for sucrose pellets in the open arena. Electrical signals were preamplified using unity gain operational amplifiers on an HS-18-MM headstage. Signals from each tetrode or stereotrode wire were then differentially referenced against a quiet channel from a separate tetrode or stereotrode and band-pass–filtered (600 Hz to 6 kHz) using a Cheetah 32 Data Acquisition System. If signals on a given tetrode or stereotrode crossed a predefined amplitude threshold (30 to 50 μV), then they were time-stamped and digitized at 32 kHz for 1 ms. The headstage was also equipped with red and green light-emitting diodes (LEDs) spaced ~6 cm apart over the head and back of the animal, respectively. A color video camera positioned over the arena captured video frames with a sampling rate of 30 Hz for POR data and 60 Hz for ATN data, and an automated video tracker extracted the x and y positions of the LEDs and their angle in an allocentric frame. The tracking frames were time-stamped so that they could be matched up to the neural data. If clearly isolated waveforms were visually apparent, then a 20-min baseline recording session in the 120-cm square box or a 10-min baseline recording session in the 100-cm square box took place. Visual cues present during these baseline sessions were the same as those used in the behavioral training sessions. If no clear waveforms were detected, then electrodes were advanced ~50 to 100 μm and screened again at least 2 hours later or the next day (*8*).

Spike sorting

Spike sorting was conducted offline. Spikes collected from a recording session were first automatically sorted into clusters using the automated clustering program Kilosort (*55*), after which manual cleanup was performed using the manual clustering program SpikeSort3D (Neuralynx). If cells were recorded across multiple sessions in a day (i.e., with multiple cue configurations), then automatic sorting was performed on a merged dataset to ensure cluster continuity, and then, results were separated into individual sessions for manual cleanup and analysis. For the manual step, waveform features including peak, valley, height, width, and principal components were used to visualize the characteristics of individual spikes across multiple wires of a tetrode or stereotrode simultaneously as a three-dimensional scatter plot. Cleanup of automatically sorted clusters, which was not always required, was performed by drawing a polygon around the visually apparent boundaries of each cluster. Single-unit isolation was assessed using metrics such as L ratio and isolation distance, as well as assessment of temporal autocorrelograms for the presence of a refractory period. Cross-correlograms were also analyzed to make sure that the same cells were not recorded across different tetrodes or stereotrodes. Despite significant advancement of the electrodes between recording sessions, we sometimes found that the same cells were recorded multiple times on the same tetrodes or stereotrodes across recording sessions (based on analyzing waveform shape and location in cluster space); in these cases, we only used the first recording session of the cell. For each well-isolated cluster, we saved the time stamps for each spike and then analyzed and matched them to the tracking data (*8*).

Cue recording sessions: One-cue condition

If an HD-responsive cell was isolated in the baseline session (classification criteria discussed below), then the cell was subsequently recorded across a number of different cue configurations. Animals were always returned to their home cage in between recording sessions, and the floor paper was always changed to reduce the presence of local cues left behind from previous sessions. As the home cage was located in a different room from the recording arena, changes made to the recording arena (such as added landmark cues) were not observed by the animals until the commencement of the following recording session. Animals were not disoriented in between sessions (except for one exception outlined below). The following sessions were run with animals initially habituated to an enclosure with a single white cue card (cue A) along the south wall (group 1 above). Sessions with different cue configurations were not always run in the same order, but they were always preceded and followed by a standard session with cue A only, except for one experiment where the AB session was followed by a No cue session and then a final A-only session (Fig. 3, J to N).

No cue session

No cue cards were present during this session. The animal was allowed to forage for sugar pellets for either a 10-min (100-cm box) or 20-min (120-cm box) recording session.

AB session
Both cue A (a white cue card placed along the south wall) and cue B (an identical white cue card placed along the north wall) were present during this session. The animal was allowed to forage for sugar pellets in the presence of both cues for either a 10-min (100-cm box) or 20-min (120-cm box) recording session.

AB_{west} session
Both cue A (a white cue card placed along the south wall) and cue B_{west} (an identical white cue card placed along the west wall) were present during this session. The animal was allowed to forage for sugar pellets in the presence of both cues for a 20-min (120-cm box) recording session.

B-only session
Only cue B (a white cue card placed along the north wall) was present during this session. The animal was allowed to forage for sugar pellets in the presence of this cue for either a 10-min (100-cm box) or 20-min (120-cm box) recording session.

AC session
Both cue A (a white cue card placed along the south wall) and cue C (a black cue card placed along the north wall) were present during this session. Both cue cards were of identical size and shape but differed in their color. The animal was allowed to forage for sugar pellets in the presence of both cues for either a 10-min (100-cm box) or 20-min (120-cm box) recording session.

Other
Some POR animals were also exposed to environments with different boundary conditions. Data from these sessions are not presented here.

Cue recording sessions: Black-cue condition
Recording sessions for the animals initially trained with other cue configurations were run similarly to those in the one-cue condition in terms of the general layout of the recording environment, handling the animals, and changing the floor paper between sessions. For animals trained with a single black cue card along the south wall, if an HD-responsive cell was identified in a baseline session with the single black cue card present (10 min for 100-cm box or 20 min for 120-cm box), then this session was followed by another foraging session in the same enclosure with an identical black cue card along the north wall and, subsequently, a final standard session with the single black cue card (A1 black–AB black–A2 black).

Cue recording sessions: Two-cue condition
For animals trained with a pair of white cue cards placed along the south (cue A) and north (cue B) walls of the enclosure, if an HD-responsive cell was identified in a baseline session with both cues present (10 min for 100-cm box or 20 min for 120-cm box), then this session was followed by another foraging session in the same enclosure with only cue A present and, subsequently, a final standard session with both cues present (AB1-A-AB2).

Cue recording sessions: No cue condition
For animals trained without any cue cards in the enclosure, if an HD-responsive cell was identified in a baseline session with no cue (10 min for 100-cm box or 20 min for 120-cm box), then this session was followed by another foraging session in the same enclosure with a pair of visually identical cue cards placed along the south (cue A) and north (cue B) walls of the enclosure and, subsequently, a final standard session with no cues present (No cue 1–AB–No cue 2). Visually distinct cue pairs were used on adjacent recording days to keep them from being established as stable visual cues. Pairs were used in the following order: (i) two white cue cards, (ii) two black cue cards, (iii) two white cue cards with horizontal black stripes, (iv) two white cue cards with vertical black stripes, (v) two cue cards that were black on the left half and white on the right half, and (vi) two cue cards that were black on the top half and white on the bottom half.

After the three initial sessions took place (i.e., after No cue 2), the pair of cues was reintroduced to the enclosure but rotated onto adjacent walls (i.e., placed along the east and west walls instead of north and south). The animal was brought into the recording environment and placed into a cardboard box, which the experimenter closed and rotated slowly while walking around the enclosure to disorient the animal. This is the only experiment where disorientation took place in between sessions. The animal was then placed into the enclosure in a random location, and a recording session was run. After this, the animal was removed and the cues were rotated back to the north and south walls, and a final recording session took place (No cue–AB rotated–AB).

Histology
Once recordings were complete, animals were deeply anesthetized with sodium pentobarbital, and small marking lesions were made at the electrode tips by passing a small anodal current (15 μA, 15 to 20 s) through two active wires from separate tetrodes or stereotrodes. Animals were then intracardially perfused with saline followed by 10% formalin solution, after which the brains were removed from the skull and postfixed in 10% formalin solution with 2% potassium ferrocyanide for at least 24 hours. The brains were then transferred to 20% sucrose solution for at least 24 hours, after which they were frozen and sliced sagittally (for postrhinal implants) or coronally (for anterior thalamus implants; 30-μm sections) using a cryostat. Sections were mounted on glass microscope slides and stained with thionin, after which electrode tracks were examined using a light microscope (fig. S14). Locations of recorded cells were determined by measuring backward from the most ventral location of the marking lesions or, if marking lesions were not visible, the electrode tracks (*8*). For one animal (PL73; fig. S14A), we could not confidently assign any cells to POR, but several HD cells recorded from the neighboring PaS or MEC were recorded and analyzed separately. Delineations of parahippocampal regions were drawn mainly from (*56*, *57*), while delineations of the anterior thalamus were drawn from (*58*).

Cell classifications with a generalized linear model
Cells were initially classified as encoding up to four behavioral variables using 10-fold cross-validation with a Poisson generalized linear model (GLM) (*8*, *59*). The behavioral variables were as follows: allocentric HD, egocentric bearing of the environment center, egocentric distance of the environment center, and linear speed. For each model, the firing rate vector r for a single cell over all time points was modeled as follows

$$r = \exp\left(\sum_i X_i^T \beta_i\right)$$

where X is a matrix containing animal state vectors for a single behavioral variable over time points T, β represents the parameter vector for that behavioral variable (similar to a tuning curve), and i indexes across behavioral variables included in the model. The parameter

vectors for a given model are learned by maximizing the log-likelihood l of the real spike train n given the model's estimated rate vector r

$$l = \sum_t n_t \log(r_t) - r_t - \log(n_t!)$$

where t indexes over time points. To avoid overfitting and potential artifacts for the cross-validation procedure, an additional smoothing penalty P was added to the objective function, which penalizes differences between adjacent bins of each parameter vector

$$P = \sum_i S \sum_j \frac{1}{2} * (\beta_{i,j+1} - \beta_{i,j})^2$$

Here, S is a smoothing hyperparameter (set to 20 for all variables), i indexes over variables, and j indexes over response parameters for a given variable. Response parameters were estimated by minimizing ($P - l$) using SciPy's optimize.minimize function. Thirty bins were used for center bearing and allocentric HD parameter vectors, and 10 bins were used for center distance and linear speed.

For cross-validation, data for a session was split into training (9 of 10) and test (1 of 10) data ($k = 10$ folds) by first splitting the session into 50 equal-length blocks, and then, for each fold, from $k = 1$ to 10, we assigned every 10th block starting with k to that fold (*59*). Parameter vectors were estimated by minimizing the objective function on the training data using the full model with all four variables. Drawing parameter estimates from the full model helps reduce correlation artifacts between variables (*60*) and makes models with different variable combinations more comparable. Log-likelihoods for models with all possible variable combinations were computed. This was repeated until all portions of the data had been used as test data (10 folds).

To select the best model, the log-likelihood values from the best two-variable model were compared to those from the best one-variable model. If the two-variable model showed significant improvement from the one-variable model (using a one-sided Wilcoxon signed-rank test), then the best three-variable model was compared to the two-variable model, and so on. If the more complex model was not significantly better, then the simpler model was chosen. If the chosen model performed significantly better than an intercept-only model, then the chosen model was used as the cell's classification. Otherwise, the cell was marked "unclassified" (*59*).

To assess the influence of each variable that a given cell was tuned to, we fit the cell's chosen model on tracking data from the whole recording session, after which we removed the variable of interest from the model and computed the change in goodness-of-fit measures. One measure was log-likelihood per spike, which was calculated by dividing the log-likelihood l by the total number of spikes fired by the cell. The other was explained variance (R^2), which was computed by binning the cells' actual spike train n and the modeled firing rate vector r into 300-ms bins and then performing the following calculation

$$R^2 = 1 - \sum_t \frac{(n_t - r_t)^2}{(n_t - \overline{n})^2}$$

where $\overline{n}$ is the mean of the actual spike train.

HD tuning curves and classification

HD tuning curves were created using 12° bins. These bins were larger than the more typical 6° bins because of the broad tuning curves of POR cells, although the overall pattern of results was the same when using 6° bins. For each cell, the amount of time that each bin was sampled and the number of spikes fired per bin over the course of a session were calculated, and the tuning curve was computed by dividing the number of spikes per bin by the amount of sampling time per bin.

The MVL and PFD of the HD tuning curve were extracted to indicate tuning strength and PFD, respectively. A neuron was considered an HD-responsive cell if it (i) passed the classification procedure for HD modulation, (ii) had MVL > 99th percentile of a within-cell shuffle distribution (discussed below), and (iii) had maximum firing rate > 1 Hz in its HD tuning curve (*8*). HD-responsive cells recorded in the POR of animals that were initially habituated to a single cue card are referred to as LM-HD cells because of their firing properties related to visual cues, while HD cells recorded from the ATN and MEC/PaS are simply referred to as HD cells. However, for HD-responsive POR cells recorded in animals that were habituated to two or no cues, we simply refer to them as HD-responsive cells because their landmark-response properties are less well defined.

Of a total of 353 recorded POR neurons from the nine rats initially habituated to a single white cue card with confirmed recordings in POR, 177 cells were identified as LM-HD cells (50%). Eighty-seven of the 177 LM-HD cells ($n = 5$ rats) were recorded in the AB experiment, and a subset of these 87 cells were also recorded across one or more of the other cue configuration sessions (45 cells in the No cue experiment, 39 cells in the B experiment, 36 cells in the AC experiment, and 49 cells in the AB_{west} experiment). Thus, all cells recorded in the No cue, B, AC, and AB_{west} experiments were also included in the AB experiment. One rat (PL86) provided a large proportion of cells in the AB experiment (52 of 87), but the bidirectional properties of these cells did not differ from LM-HD cells recorded from the other rats (Welch's t test for BI, $t_{80} = -1.77$, $P = 0.082$).

Following the completion of these experiments, three additional rats (91, 92, and 93; fig. S14B) were trained in the same fashion with a single white cue card, and 47 of 145 POR cells were found to be LM-HD cells (32%). Twenty-seven of these cells were recorded in the following session order: A1, AB, No cue, and A2 (Fig. 3, J to N).

Normalized HD tuning curves

HD tuning curves for individual cells were sorted according to their PFDs; their firing rates were normalized and plotted as a heatmap. Normalized tuning curves visualized across multiple recording sessions were sorted according to the cells' PFDs in the first session, and their firing rates were normalized according to the minimum and maximum firing rates observed across all visualized sessions.

Assessment of bidirectionality

Bidirectionality of HD tuning was assessed for a particular cell by computing its angle-doubled tuning curve (*28*, *33*). Angle doubling (multiplying all angles by 2) has the advantage of turning a bidirectional distribution (two peaks separated by 180°) into a unidirectional one. HDs for a single recording session were doubled, and 360° was subtracted from values exceeding 360°. Tuning curves were then computed normally using these doubled angles, and the MVL and PFD were extracted. The angle-doubled MVL was then compared to the normally computed MVL for the same cell to derive a BI

$$BI = (MVL_{doubled} - MVL_{normal})/(MVL_{doubled} + MVL_{normal})$$

Changes in bidirectionality in a given recording session compared to the preceding baseline session were plotted as the increase in BI for the session of interest compared to the preceding baseline session

$$\Delta BI = BI_{experimental} - BI_{baseline}$$

Assessment of peak-locked and trough-locked tuning

Bidirectional tuning curves from the AB session revealed that some POR LM-HD cells anchored their firing rate maxima to the location of a visual cue, increasing their firing rates when the animal was facing in the general direction of a cue, which we termed peak-locked tuning. The AB tuning curves for peak-locked cells showed a peak at the original A1 PFD and a second peak 180° opposite. However, other cells instead showed anchoring of their firing rate minima, apparently reducing their firing rates when the animal was facing in the general direction of a cue, which we termed trough-locked tuning. The AB tuning curves for trough-locked cells appeared to have two peaks that were displaced 90° clockwise and counterclockwise from the A1 PFD. Whether the AB peaks were aligned or displaced (reflecting peak or trough locking, respectively) compared to the A1 PFD could be assessed by doubling the A1 PFD (and subtracting 360° if the result exceeded 360°) and comparing it to the angle-doubled PFD from the AB session

$$\text{Peak displacement} = (2 \times PFD_{A1})\ \%360 - PFD_{doubled\_AB}$$

If they were aligned (i.e., displacement near 0°), then it suggested that the PFD from the A1 session was retained during the AB session and a second peak was added 180° opposite. If the displacement was closer to 180°, however, then it suggested that the original PFD from A1 was displaced by a new firing rate minimum. Note that the peak displacement expected for trough-locked tuning is 180° instead of 90° because of the angle doubling. We used this difference measure to confirm that the clusters derived from the PCA and von Mises fit procedures (discussed below) corresponded to peak-locked and trough-locked cells.

Principal components analysis

To determine whether peak-locked or trough-locked tuning in the AB session could be determined from the cells' A1 tuning curves, we performed a PCA (from Python's scikit-learn library) on all of the normalized A1 tuning curves of cells recorded in the AB condition. The first component (PC1) explained much of the tuning curve variance and appeared to separate cells into two distinct clusters on the basis of whether they had peaks or troughs near 270°. We performed *k*-means clustering (also from Python's scikit-learn library) using the first two components, which confirmed the visually distinct clusters. We then confirmed that these two clusters represented peak-locked and trough-locked cells by computing their peak displacements between A1 and AB sessions (discussed above).

Standard and inverted von Mises fits

LM-HD cells that showed peak-locked tuning in the AB session tended to show a sharp peak at their PFD during the A1 session, while LM-HD cells revealed to be trough-locked in the AB session tended to show a sharper trough 180° opposite their A1 PFD. To assess this distinction, we fit both a von Mises distribution (sharp peak) and an inverted von Mises distribution (sharp trough) to each HD tuning curve from the A1 session and computed the difference in R^2 fit values ($R^2_{standard} - R^2_{inverted}$). Cells were separated into two groups using *k*-means clustering based on these R^2 differences and the A1 PFDs. PFDs were separated into *x* and *y* components to retain the circular nature of the data for the *k*-means algorithm. We compared the resulting clusters to those derived from the PCA to confirm that they were identical and therefore represented peak-locked and trough-locked cells.

Cue modulation measures

To assess the degree of firing rate modulation attributable to each cue during the AB, B, and AC conditions, we fit a bimodal (separated by 180°) von Mises distribution (standard for peak-locked and inverted for trough-locked cells) to each cell's HD tuning curve from the relevant experimental session. Modulation by cue A was computed by first finding the von Mises peak or trough that most closely matched the cell's A1 tuning curve and then calculating the difference in firing rate between that peak or trough and the minimum or maximum firing rate of the fit curve, respectively. This firing rate difference was transformed into an MI (similar to a signal-to-noise ratio) by dividing it by the maximum firing rate of the fit curve (where fr is firing rate)

$$MI_A = (\text{peak fr}_A - \text{min fr (fit curve)})/\text{max fr (fit curve)}\ \text{[for peak-locked cells]}$$

or

$$MI_A = (\text{max fr (fit curve)} - \text{trough fr}_A)/\text{max fr (fit curve)}\ \text{[for trough-locked cells]}$$

where the subscript A indicates the portion of the tuning curve attributed to cue A. The MI for cue B (or C) was then calculated by performing the same computation on the peak or trough 180° opposite. For the AB_{west} session, this analysis was performed using a bimodal distribution with modes separated by 90°.

For the No cue, A1, and A2 conditions, we fit a single von Mises distribution to the tuning curve and performed the same calculations to derive the MI for cue A only. MI values could range from 0 to 1 for each cue, with a value of 0 indicating that no firing rate modulation occurred with respect to that cue (i.e., the portion of the cell's tuning curve attributed to that cue was completely flat) and a value of 1 indicating that the cell's firing rate was maximally modulated with respect to that cue (i.e., the portion of the cell's tuning curve attributed to that cue ranged from 0 spikes/s to the cell's peak firing rate). For the AB_{west} session, we also fit a unimodal distribution to the A1, AB_{west}, and A2 curves and extracted the concentration parameter κ as a measure of tuning width.

Change in bidirectionality with repeated exposures to AB session

To test whether the LM-HD cells became less bidirectionally modulated with repeated exposures to the AB session, we used a linear mixed model (Python's statsmodels.formula.api.mixedlm) to determine the influence of the number of exposures to AB on ΔBI for all LM-HD cells recorded in the AB experiment. Because different animals contributed different numbers of LM-HD cells and experienced different numbers of exposures, we limited our data to animals that had at least two exposures to the AB session ($n = 4$ of 5 animals used in the AB experiment) and allowed the model to estimate individual slopes and intercepts for each animal

$$\Delta BI \sim \text{Exposure} + (1 + \text{Exposure} \mid \text{Animal})$$

Tuning curve cross-correlations

To look for changes in tuning preferences between two recording sessions, in some cases, we performed angular cross-correlations between the HD tuning curves of individual cells recorded in both sessions. The first value of the cross-correlation (at an angular offset of 0°) was computed by aligning the two tuning curves for a single cell and computing Pearson's *r*. After this, the first tuning curve was circularly shifted relative to the second tuning curve in 12° increments, and Pearson's *r* was calculated at every angular offset up to 360°, until correlation values had been obtained for all possible offsets. We then calculated the mean and SEM for each angular offset across all relevant cells, which were used for plotting.

Allocentric position firing rate maps

The animal's two-dimensional location throughout the recording session was divided into 4 cm–by–4 cm bins. For each cell, the number of spikes fired when the animal occupied each bin was divided by the amount of time the animal spent in that bin to calculate a firing rate for each location in the environment. The resulting firing rate heatmaps were smoothed with a Gaussian filter (*8*).

Spatial information content

Modulation of each cell's firing rate by the animal's allocentric position was assessed by computing the spatial information content of its smoothed firing rate heatmap, computed using the following formula (*61*)

$$\sum_i p_i \frac{r_i}{\bar{r}} \log_2 \frac{r_i}{\bar{r}}$$

where i indexes across spatial bins, p_i denotes the animal's probability of occupying bin i over the course of the session, r_i denotes the firing rate in bin i of the heatmap, and $\bar{r}$ denotes the overall mean firing rate. Cells were considered to be spatially modulated if they passed a 99th percentile shuffle cutoff for spatial information content.

Border score

Smoothed firing rate heatmaps were first thresholded to only include bins higher than 20% of each cell's maximum firing rate. Firing fields were defined as above-threshold contiguous groups of bins with size >200 cm^2. We next determined the firing field with the most bins along one wall of the enclosure and converted that number of bins into a distance along that wall, *d*. We then calculated the average distance of each of the bins in that firing field from the associated wall, *a*. The border score, *B*, was then computed according to the following equation (*8*, *32*)

$$B = (d–a)/(d + a)$$

Cells that passed a 99th percentile shuffle cutoff for both spatial information content and border score were considered border cells.

Directional spike plots

To visualize the directional firing of cells across space, we created directional spike plots that plot the path taken by the animal during foraging (gray trace) overlaid with dots indicating the animal's location when a single cell fired a spike. The dots are colored (circular rainbow color palette) according to the animal's allocentric HD when the spike was fired: red, 0°; green, 90°; blue, 180°; and purple, 270° (*8*).

Shuffling procedure

Each cell's spike train was randomly shifted by at least 30 s, with entries beyond the end wrapped to the beginning, to offset the spike data from the behavioral data without interrupting its temporal structure. Relevant tuning scores were then computed on the basis of the shifted spike train (*8*). This procedure was repeated 400 times for each cell, and a within-cell 99th percentile cutoff was used to determine tuning significance for individual cells.

Statistics

Statistical analyses were performed using Python code. All tests were two sided (except for GLM classifier cross-validation comparisons) (*8*, *59*) and used an α level of 0.05. A circular *V* test was used to test for concentration of PFD shifts around a predicted value, whereas the Rayleigh statistic was used to assess general clustering of angular shifts (*62*, *63*). A circular correlation statistic was also used to assess relationships between angular variables (*64*). Nonangular within-cell comparisons across multiple conditions were assessed using a one-way repeated-measures ANOVA. If samples violated sphericity (assessed using Mauchly's test), then we applied a Greenhouse-Geisser correction. Post hoc pairwise comparisons were performed using Bonferroni-corrected paired *t* tests. Differences between the distributions of BIs for animals trained with one versus two white cue cards were assessed using a Mann-Whitney *U* test. Chi-square tests were used to compare proportions using a contingency table.

SUPPLEMENTARY MATERIALS

Supplementary material for this article is available at https://science.org/doi/10.1126/sciadv.abg8404

View/request a protocol for this paper from *Bio-protocol*.

REFERENCES AND NOTES

1. C. R. Gallistel, *The Organization of Learning* (Bradform Books/MIT, 1990).
2. J. S. Taube, R. U. Muller, J. B. Ranck Jr., Head-direction cells recorded from the postsubiculum in freely moving rats. I. Description and quantitative analysis. *J. Neurosci.* **10**, 420–435 (1990).
3. R. W. Stackman, J. S. Taube, Firing properties of head direction cells in the rat anterior thalamic nucleus: Dependence on vestibular input. *J. Neurosci.* **17**, 4349–4358 (1997).
4. J. P. Goodridge, P. A. Dudchenko, K. A. Worboys, E. J. Golob, J. S. Taube, Cue control and head direction cells. *Behav. Neurosci.* **112**, 749–761 (1998).
5. J. S. Taube, R. U. Muller, J. B. Ranck Jr., Head-direction cells recorded from the postsubiculum in freely moving rats. II. Effects of environmental manipulations. *J. Neurosci.* **10**, 436–447 (1990).
6. J. J. Knierim, H. S. Kudrimoti, B. L. McNaughton, Place cells, head direction cells, and the learning of landmark stability. *J. Neurosci.* **15**, 1648–1659 (1995).
7. L. Nadel, J. Willner, Context and conditioning: A place for space. *Physiol. Psychol.* **8**, 218–228 (1980).
8. P. A. LaChance, T. P. Todd, J. S. Taube, A sense of space in postrhinal cortex. *Science* **365**, eaax4192 (2019).
9. X. Gofman, G. Tocker, S. Weiss, C. N. Boccara, L. Lu, M.-B. Moser, E. I. Moser, G. Morris, D. Derdikman, Dissociation between postrhinal cortex and downstream parahippocampal regions in the representation of egocentric boundaries. *Curr. Biol.* **29**, 2751–2757.e4 (2019).
10. O. Kornienko, P. Latuske, B. Bassler, L. Kohler, K. Allen, Non-rhythmic head-direction cells in the parahippocampal region are not constrained by attractor network dynamics. *eLife* **7**, e35949 (2018).
11. R. D. Burwell, M. P. Witter, D. G. Amaral, Perirhinal and postrhinal cortices of the rat: A review of the neuroanatomical literature and comparison with findings from the monkey brain. *Hippocampus* **5**, 390–408 (1995).
12. G. K. Aguirre, J. A. Detre, D. C. Alsop, M. D'Esposito, The parahippocampus subserves topographical learning in man. *Cereb. Cortex* **6**, 823–829 (1996).
13. G. K. Aguirre, M. D'Esposito, Topographical disorientation: A synthesis and taxonomy. *Brain* **122**, 1613–1628 (1999).
14. R. Epstein, N. Kanwisher, A cortical representation of the local visual environment. *Nature* **392**, 598–601 (1998).

15. G. Janzen, M. van Turennout, Selective neural representation of objects relevant for navigation. *Nat. Neurosci.* **7**, 673–677 (2004).
16. R. D. Burwell, D. M. Hafeman, Positional firing properties of postrhinal cortex neurons. *Neuroscience* **119**, 577–588 (2003).
17. S. C. Furtak, O. J. Ahmed, R. D. Burwell, Single neuron activity and theta modulation in postrhinal cortex during visual object discrimination. *Neuron* **76**, 976–988 (2012).
18. K. L. Agster, R. D. Burwell, Cortical efferents of the perirhinal, postrhinal, and entorhinal cortices of the rat. *Hippocampus* **19**, 1159–1186 (2009).
19. R. D. Burwell, D. G. Amaral, Cortical afferents of the perirhinal, postrhinal, and entorhinal cortices of the rat. *J. Comp. Neurol.* **398**, 179–205 (1998).
20. K. L. Agster, R. D. Burwell, Hippocampal and subicular efferents and afferents of the perirhinal, postrhinal, and entorhinal cortices of the rat. *Behav. Brain Res.* **254**, 50–64 (2013).
21. R. D. Burwell, D. G. Amaral, Perirhinal and postrhinal cortices of the rat: Interconnectivity and connections with the entorhinal cortex. *J. Comp. Neurol.* **391**, 293–321 (1998b).
22. I. T. Pereira, K. L. Agster, R. D. Burwell, Subcortical connections of the perirhinal, postrhinal, and entorhinal cortices of the rat. I. afferents. *Hippocampus* **26**, 1189–1212 (2016).
23. R. Beltramo, M. Scanziani, A collicular visual cortex: Neocortical space for an ancient midbrain visual structure. *Science* **363**, 64–69 (2019).
24. J. S. Taube, Head direction cells recorded in the anterior thalamic nuclei of freely moving rats. *J. Neurosci.* **15**, 70–86 (1995).
25. M. Tsanov, E. Chah, S. D. Vann, R. B. Reilly, J. T. Erichsen, J. P. Aggleton, S. M. O'Mara, Theta-modulated head direction cells in the rat anterior thalamus. *J. Neurosci.* **31**, 9489–9502 (2011).
26. A. Bicanski, N. Burgess, Environmental anchoring of head direction in a computational model of retrosplenial cortex. *J. Neurosci.* **36**, 11601–11618 (2016).
27. H. J. I. Page, K. J. Jeffery, Landmark-based updating of the head direction system by retrosplenial cortex: A computational model. *Front. Cell. Neurosci.* **12**, 191 (2018).
28. P.-Y. Jacob, G. Casali, L. Spieser, H. Page, D. Overington, K. Jeffery, An independent, landmark-dominated head-direction signal in dysgranular retrosplenial cortex. *Nat. Neurosci.* **20**, 173–175 (2017).
29. C. Wang, X. Chen, H. Lee, S. S. Deshmukh, D. Yoganarasimha, F. Savelli, J. J. Knierim, Egocentric coding of external items in the lateral entorhinal cortex. *Science* **362**, 945–949 (2018).
30. A. S. Alexander, L. C. Carstensen, J. R. Hinman, F. Raudies, G. W. Chapman, M. E. Hasselmo, Egocentric boundary vector tuning of the retrosplenial cortex. *Sci. Adv.* **6**, eaaz2322 (2020).
31. J. O'Keefe, L. Nadel, *The Hippocampus as a Cognitive Map* (Oxford Univ. Press, 1978).
32. T. Solstad, C. N. Boccara, E. Kropff, M.-B. Moser, E. I. Moser, Representation of geometric borders in the entorhinal cortex. *Science* **322**, 1865–1868 (2008).
33. Y. R. Lozano, H. Page, P.-Y. Jacob, E. Lomi, J. Street, K. Jeffery, Retrosplenial and postsubicular head direction cells compared during visual landmark discrimination. *Brain Neurosci. Adv.* **1**, 2398212817721859 (2017).
34. J. P. Goodridge, J. S. Taube, Preferential use of the landmark navigational system by head direction cells in rats. *Behav. Neurosci.* **109**, 49–61 (1995).
35. R. N. Ramesh, C. R. Burgess, A. U. Sugden, M. Gyetvan, M. L. Andermann, Intermingled ensembles in visual association cortex encode stimulus identity or predicted outcome. *Neuron* **100**, 900–915.e9 (2018).
36. A. A. Wilber, B. J. Clark, T. C. Forster, M. Tatsuno, B. L. McNaughton, Interaction of egocentric and world-centered reference frames in the rat posterior parietal cortex. *J. Neurosci.* **34**, 5431–5446 (2014).
37. Y. Yan, N. Burgess, A. Bicanski, A model of head direction and landmark coding in complex environments. *PLoS Comput. Biol.* **17**, e1009434 (2021).
38. N. Sethumadhavan, T.-H. Hoang, C. Strauch, D. Manahan-Vaughan, Involvement of the postrhinal and perirhinal cortices in microscale and macroscale visuospatial information encoding. *Front. Behav. Neurosci.* **14**, 556645 (2020).
39. D. J. Bucci, R. G. Phillips, R. D. Burwell, Contributions of postrhinal and perirhinal cortex to contextual information processing. *Behav. Neurosci.* **114**, 882–894 (2000).
40. D. J. Bucci, M. P. Saddoris, R. D. Burwell, Contextual fear discrimination is impaired by damage to the postrhinal or perirhinal cortex. *Behav. Neurosci.* **116**, 479–488 (2002).
41. M. Fyhn, T. Hafting, A. Treves, M.-B. Moser, E. I. Moser, Hippocampal remapping and grid realignment in entorhinal cortex. *Nature* **446**, 190–194 (2007).
42. D. J. Bucci, R. D. Burwell, Deficits in attentional orienting following damage to the perirhinal or postrhinal cortices. *Behav. Neurosci.* **118**, 1117–1122 (2004).
43. M. Davies, P. E. Machin, D. J. Sanderson, J. M. Pearce, J. P. Aggleton, Neurotoxic lesions of the rat perirhinal and postrhinal cortices and their impact on biconditional visual discrimination tasks. *Behav. Brain Res.* **176**, 274–283 (2007).
44. G. Zhang, H. Cao, L. Kong, J. O'Brien, A. Baughns, M. Jan, H. Zhao, X. Wang, X. Lu, R. Cook, A. I. Geller, Identified circuit in rat postrhinal cortex encodes essential information for performing specific visual shape discriminations. *Proc. Natl. Acad. Sci. U.S.A.* **107**, 14478–14483 (2010).
45. A. A. Kinkhabwala, Y. Gu, D. Aronov, D. W. Tank, Visual cue-related activity of cells in the medial entorhinal cortex during navigation in virtual reality. *eLife* **9**, e43140 (2020).
46. G. Casali, S. Shipley, C. Dowell, R. Hayman, C. Barry, Entorhinal neurons exhibit cue locking in rodent VR. *Front. Cell. Neurosci.* **12**, 512 (2019).
47. J. A. Perez-Escobar, O. Kornienko, P. Latuske, L. Kohler, K. Allen, Visual landmarks sharpen grid cell metric and confer context specificity to neurons of the medial entorhinal cortex. *eLife* **5**, e16937 (2016).
48. L. Acharya, Z. M. Aghajan, C. Vuong, J. J. Moore, M. R. Mehta, Causal influence of visual cues on hippocampal directional selectivity. *Cell* **164**, 197–207 (2016).
49. J. R. Peck, J. S. Taube, The postrhinal cortex is not necessary for landmark control in rat head direction cells. *Hippocampus* **27**, 156–168 (2017).
50. J. P. Goodridge, J. S. Taube, Interaction between postsubiculum and anterior thalamus in the generation of head direction cell activity. *J. Neurosci.* **17**, 9315–9330 (1998).
51. R. M. Yoder, B. J. Clark, J. S. Taube, Origins of landmark encoding for the brain's navigation system. *Trends in Neurosci.* **34**, 561–571 (2011).
52. J. O'Keefe, An allocentric spatial model for the hippocampal cognitive map. *Hippocampus* **1**, 230–235 (1991).
53. A. P. Duchon. Maze navigation using optical flow, in *From Animals to Animats 4: Proceedings of the Fourth International Conference on Adaptive Behavior*, P. Maes, M. J. Mataric, J.-A. Meyer, J. Pollack, S. W. Wilson, Eds. (MIT Press/Bradford Books, 1996), pp. 224–232.
54. L. Kunz, A. Brandt, P. C. Reinacher, B. P. Staresina, E. T. Reifenstein, C. T. Weidemann, N. A. Herweg, A. Patel, M. Tsitsiklis, R. Kempter, M. J. Kahana, A. Schulze-Bonhage, J. Jacobs, A neural code for egocentric spatial maps in the human medial temporal lobe. *Neuron* **109**, 2781–2796.e10 (2021).
55. M. Pachitariu, N. A. Steinmetz, S. Kadir, M. Carandini, K. D. Harris, Fast and accurate spike sorting of high-channel count probes with Kilosort. *Adv. Neural Inf. Proces. Syst.* **29**, 4448–4456 (2016).
56. C. N. Boccara, L. J. Kjonigsen, I. M. Hammer, J. G. Bjaalie, T. B. Leergaard, M. P. Witter, A three-plane architectonic atlas of the rat hippocampal region. *Hippocampus* **25**, 838–857 (2015).
57. R. D. Burwell, Borders and cytoarchitecture of the perirhinal and postrhinal cortices in the rat. *J. Comp. Neurol.* **437**, 17–41 (2001).
58. G. Paxinos, C. Watson, *The Rat Brain in Stereotaxic Coordinates* (Academic Press, ed. 4, 1998).
59. K. Hardcastle, N. Maheswaranathan, S. Ganguli, L. M. Giocomo, A multiplexed, heterogeneous, and adaptive code for navigation in medial entorhinal cortex. *Neuron* **94**, 375–387.e7 (2017).
60. N. Burgess, F. Cacucci, C. Lever, J. O'Keefe, Characterizing multiple independent behavioral correlates of cell firing in freely moving animals. *Hippocampus* **15**, 149–153 (2005).
61. E. J. Markus, C. A. Barnes, B. L. McNaughton, V. L. Gladden, W. E. Skaggs, Spatial information content and reliability of hippocampal CA1 neurons: Effects of visual input. *Hippocampus* **4**, 410–421 (1994).
62. E. Batschelet, *Circular Statistics in Biology* (Academic Press, 1981).
63. K. V. Mardia, P. E. Jupp, *Directional Statistics* (Wiley, 2000).
64. S. R. Jammalamadaka, A. Sengupta, *Topics in Circular Statistics* (World Scientific, 2001).

Acknowledgments: We thank J. L. Marcroft for technical assistance and performing some of the experiments. **Funding:** This work was supported by NIH grants NS053907 and DC009318 awarded to J.S.T. **Author contributions:** P.A.L. and J.S.T. conceived the project and designed experiments and analyses. P.A.L. and J.G. performed surgeries. P.A.L., J.G., B.L.S., and A.J.M. ran the experiments. P.A.L. ran the analyses. P.A.L. and J.S.T. discussed the analyses and wrote the manuscript. **Competing interests:** The authors declare that they have no competing interests. **Data and materials availability:** All data needed to evaluate the conclusions of the paper are present in the paper and/or the Supplementary Materials. Code for GLM classification of POR cells is published in an online repository (https://zenodo.org/record/3173242#.YWnzvGZKjlx).

Submitted 30 January 2021
Accepted 7 December 2021
Published 28 January 2022
10.1126/sciadv.abg8404